nature cardiovascular research

ARTICLES

https://doi.org/10.1038/s44161-022-00057-1

Check for updates

Metabolic characterization of hypertrophic cardiomyopathy in human heart

Wenmin Wang[1,2,15], Jizheng Wang[3,15]✉, Ke Yao[1,2,15], Shuiyun Wang[4,15], Meng Nie[1], Yizi Zhao[1,2], Bohong Wang[1], Huanhuan Pang[1], Jingjing Xu[5], Guixin Wu[3,6], Minjie Lu[3], Nan Tang[7], Chunmei Qi[7], Hengzhi Pei[8], Xufang Luo[9], Dongsheng Li[9], Tianshu Yang[2,10], Qing Sun[11], Xiang Wei[12,13], Yan Li[11], Dingsheng Jiang[12,13], Peng Li[2,10,14], Lei Song[3,6]✉ and Zeping Hu[1]✉

Hypertrophic cardiomyopathy (HCM) is a common inherited cardiovascular disease with heterogeneous clinical presentations, governed by multiple molecular mechanisms. Metabolic perturbations underlie most cardiovascular diseases; however, the metabolic alterations and their function in HCM are unknown. Here, we describe the metabolome and lipidome of heart and plasma samples from individuals with and without HCM. Correlation analyses showed strong association between metabolic alterations and cardiac function and prognosis of patients with HCM. Using machine learning we identified metabolite panels as potential HCM diagnostic markers or predictors of survival. Clustering based on metabolome and lipidome of heart enabled stratification of patients with HCM into three subgroups with distinct cardiac function and survival. Integration of metabolomics and proteomics data identified metabolic pathways significantly altered in patients with HCM, with the pentose phosphate pathway and oxidative stress being particularly upregulated. Thus, targeting the pentose phosphate pathway and oxidative stress may serve as potential therapeutic strategies for HCM.

HCM, one of the most common inherited cardiovascular diseases, has a prevalence of up to 1:500 in the general population and affects approximately 20 million people globally[1–3]. HCM has emerged as an important cause of sudden cardiac death (particularly in adolescents and athletes), heart failure and atrial fibrillation[4,5], thus exerting a large burden on the healthcare system and economy in modern society[3]. HCM is characterized clinically by left ventricular hypertrophy (left ventricular wall thickness ≥15 mm), nondilated left ventricle and preserved or increased ejection fraction and pathologically by marked myocyte enlargement and disarray as well as interstitial fibrosis[6].

Over the last three decades, HCM is widely considered as an autosomal dominant disease mainly caused by sarcomere gene mutations and approximately 60% of patients with HCM carry pathogenic genes[6,7]. Presently, most of the reported potential pathogenic mechanisms of HCM are associated with gene mutations. For example, sarcomere associated gene mutations impair myofibrillar contractile function and disorder calcium cycling or sensitivity, resulting in compensatory hypertrophy, interstitial fibrosis and diastolic dysfunction[8,9]. However, gene mutations alone are insufficient to interpret overall clinical and pathological features of HCM[10]. Moreover, known pathogenic genes are absent in about 40% of patients with HCM and some pathogenic genes carriers live to advanced ages without developing HCM[11,12]. Therefore, it is particularly important to investigate the pathogenesis of HCM more comprehensively from new perspectives beyond gene mutations, which may promote the development of new therapeutic strategies.

Metabolism responds to multiple pathogenic factors, including genetic mutations, gut microbes and environment[13,14]. Study of metabolites in an omics manner (metabolomics and lipidomics) shows great potential in the identification of therapeutic targets, diagnosis of diseases and patient stratification in a heterogeneous patient population[15–17]. Systemic and myocardial metabolism disturbances are associated with numerous cardiovascular diseases, such as coronary artery disease, heart failure and hypertension[18,19]. However, our understanding on the global metabolic alterations in HCM is still limited.

Herein, by using targeted metabolomics and lipidomics, we identify the metabolic landscape of heart tissue and plasma samples from patients with HCM. Correlation analyses reveal that a substantial number of metabolites exhibit significant correlations with cardiac function and survival outcomes. We identify metabolite panels that may serve as diagnostic tools for HCM and predictors of survival. Consensus clustering of metabolomics and lipidomics identifies three distinct metabolic subgroups, which show distinct New York Heart Association (NYHA) class and survival outcomes.

[1]School of Pharmaceutical Sciences, Tsinghua-Peking Center for Life Sciences, Beijing Frontier Research Center for Biological Structure, Tsinghua University, Beijing, China. [2]Shanghai Qi Zhi Institute, Shanghai, China. [3]State Key Laboratory of Cardiovascular Disease, Fuwai Hospital, National Center for Cardiovascular Diseases, Chinese Academy of Medical Sciences and Peking Union Medical College, Beijing, China. [4]Department of Cardiac Surgery, Fuwai Hospital, National Center for Cardiovascular Diseases, Chinese Academy of Medical Sciences and Peking Union Medical College, Beijing, China. [5]Waters Corporation (China), Beijing, China. [6]Clinical Research Center for Cardiovascular Diseases, Fuwai Hospital, National Center for Cardiovascular Diseases, Chinese Academy of Medical Sciences and Peking Union Medical College, Beijing, China. [7]The Second Affiliated Hospital of Xuzhou Medical University, Xuzhou, China. [8]School of Computer Science, University of Illinois Urbana Champaign, Champaign, IL, USA. [9]Microsoft Research Asia, Shanghai, China. [10]Institute of Metabolism and Integrative Biology, Fudan University, Shanghai, China. [11]Institute of Biophysics, Chinese Academy of Science, Beijing, China. [12]Division of Cardiothoracic and Vascular Surgery, Tongji Hospital, Tongji Medical College, Huazhong University of Science and Technology, Wuhan, China. [13]Key Laboratory of Organ Transplantation, Ministry of Education, Chinese Academy of Medical Sciences, Wuhan, China. [14]School of Life Sciences, Tsinghua University, Beijing, China. [15]These authors contributed equally: Wenmin Wang, Jizheng Wang, Ke Yao, Shuiyun Wang. ✉e-mail: jzwang@hotmail.com; songlqd@126.com; zeping_hu@tsinghua.edu.cn

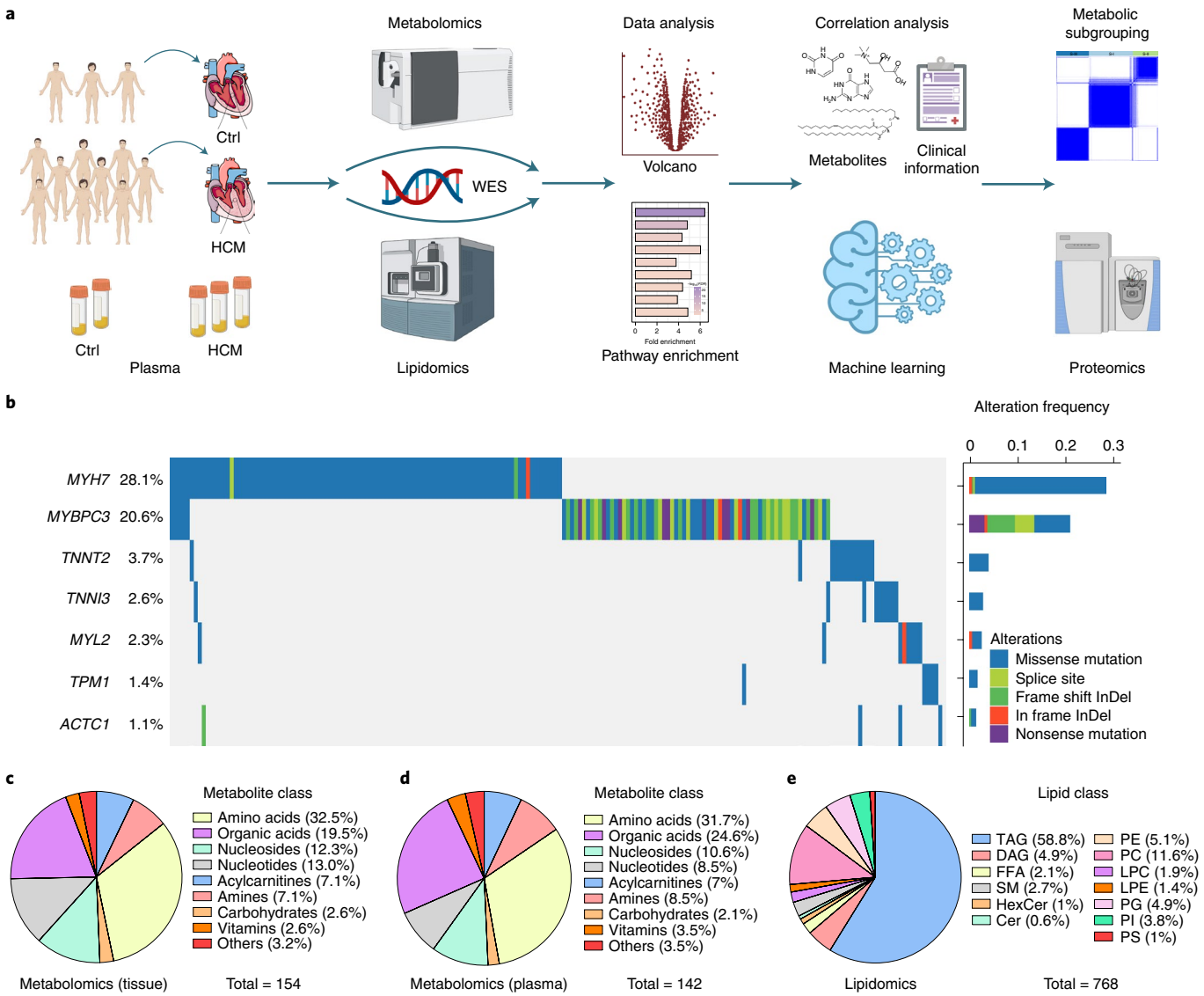

Fig. 1 | Genomic and metabolic landscape of the HCM cohort. a, Overview of the study design. The illustration was created using https://biorender.com/. Ctrl, control. **b**, Genetic profile of patients with HCM (left). Mutation types and their frequencies were showed in the right panel. *MYH7*, myosin heavy chain 7; *MYBPC3*, myosin-binding protein C 3; *TNNT2*, cardiac troponin I 2; *TNNT3*, cardiac troponin I 3; *MYL2*, myosin light chain 2; *TPM1*, α-tropomyosin 1; *ACTC1*, cardiac α-actin 1. **c**–**e**, Counts and class of metabolites detected by targeted metabolomics in cardiac tissues (**c**), plasma (**d**) and metabolites detected by lipidomics (**e**). TAG, triacylglycerol; DAG, diacylglycerol; FFA, free fatty acid; SM, sphingomyelin; HexCer, hexosylceramide; Cer, ceramide; PE, phosphatidylethanolamine; PC, phosphatidylcholine; LPC, lysophosphatidylcholine; LPE, lysophosphatidylethanolamine; PG, phosphatidylglycerol; PI, phosphatidylinositol; PS, phosphatidylserine.

By proteomics and metabolomics integrative analysis, we reveal significantly altered metabolic pathways and suggest that intervening with the pentose phosphate pathway (PPP) and oxidative stress may serve as potential therapeutic strategies for HCM. Overall, this study provides an valuable resource that expands our understanding of the metabolic alterations in patients with HCM and suggests that metabolic changes may facilitate the diagnosis, prognosis, prediction and stratification of patients with HCM. In addition, the metabolic interventions may be exploited as potential strategies for HCM treatment.

Results

Cohort characteristics and metabolic landscape of patients with HCM. To explore the global metabolic alterations in the heart and plasma samples from patients with HCM, we performed targeted metabolomics and lipidomics analyses on the human left ventricular cardiac tissues collected from 349 patients with HCM and 16 non-HCM controls, as well as metabolomics analysis on the plasma collected from 143 patients with HCM and 60 non-HCM controls (Fig. 1a). Whole-exome sequencing (WES) was carried out to detect genetic variants in eight sarcomere pathogenic genes of HCM. Correlation analyses between metabolites and clinical characteristics were applied to investigate the potential regulatory role of metabolism in HCM. In addition, machine-learning algorithms were applied to select metabolites that can precisely diagnose HCM and predict the survival outcomes of patients with HCM. Consensus clustering was performed to determine whether metabolism is a viable framework for patient classification in HCM. Proteomics was also performed to facilitate the understanding of the metabolic alterations in patients with HCM from protein level (Fig. 1a). In our cohort, all patients were diagnosed with cardiac hypertrophy by echocardiography and/or cardiovascular magnetic

resonance (Extended Data Fig. 1a). WES data showed that 202 (58%) patients with HCM carried pathogenic mutations, with myosin heavy chain 7 (*MYH7*) and myosin-binding protein C 3 (*MYBPC3*) the most common pathogenic genes as expected (Fig. 1b)[6,7]. Targeted metabolomics detected 154 metabolites in heart tissues and 142 metabolites in plasma and detected metabolites were mainly composed of amino acids, organic acids, nucleosides, nucleotides and acylcarnitines (Fig. 1c,d), which are essential for cell growth and energy metabolism[20]. Lipidomics detected a total of 768 lipids, which belong to 13 distinct lipid classes (Fig. 1e). The high quality of metabolomics and lipidomics data was confirmed by the absence of batch effects and consistency of quality control (QC) samples (Extended Data Fig. 1b–e). A total of 98% of metabolites in heart tissues and 100% metabolites in plasma detected by targeted metabolomics and 97% of lipids showed a coefficient of variation below 20% across QC samples (Extended Data Fig. 1c–e).

Metabolomics perturbations in heart tissues from patients with HCM. To identify the metabolic disturbances of patients with HCM and determine whether they share the alterations with the patients of dilated cardiomyopathy (DCM), another inherited cardiomyopathy defined by an enlarged left ventricular chamber[21], we also collected heart tissue samples from 46 patients with DCM and performed a targeted metabolomics analysis. Heat map and principal-component analysis (PCA) clearly distinguished HCM from non-HCM controls and patients with DCM (Extended Data Fig. 2a,b). A clear segregation between non-HCM controls and patients with DCM was also observed (Extended Data Fig. 2b). We found that there were 18 common upregulated (false discovery rate (FDR)-corrected $P<0.05$, fold change >1.5) and 13 common downregulated (FDR-corrected $P<0.05$, fold change <0.67) metabolites between patients with HCM and DCM compared to non-HCM controls (Extended Data Fig. 2c). Volcano plot highlighted 60 differential metabolites (36 upregulated and 24 downregulated) between patients with HCM and non-HCM controls (Fig. 2a). Notably, we found that most of the detected metabolites related to carnitine synthesis were significantly downregulated both in patients with HCM and DCM (Fig. 2b), indicating that fewer fatty acyls entered into the mitochondria for β-oxidation[22].

To characterize the dysregulated metabolic pathways in patients with HCM, we performed pathway enrichment analysis of the differential metabolites and observed that purine and pyrimidine metabolism, cysteine and methionine metabolism, vitamin B6 metabolism and glucose-related metabolic pathways were significantly perturbed in patients with HCM (Fig. 2c). Specifically, the level of *S*-adenosylmethionine (SAM), a donor for DNA and protein methylation[23], was reduced and SAM/*S*-adenosylhomocysteine (SAH) ratio was also significantly downregulated, which indicates the methylation levels were disturbed in patients with HCM (Fig. 2d). Notably, pyridoxal 5′-phosphate (PLP) and pyridoxamine that were involved in vitamin B6 metabolism displayed significant upregulation in patients with HCM (Fig. 2e). The upregulation of PLP, serving as a cofactor involved in more than 150 enzymatic reactions, may support the enlargement of cardiomyocytes[24]. Previous findings suggested that the oxidative stress was enhanced in HCM and the ratio of glutathione (GSH) to oxidized glutathione (GSSG) was significantly decreased in HCM animal models[25,26]. Our results showed that the level of GSSG was significantly upregulated both in patients with HCM and DCM, whereas the ratio of GSH/GSSG was only significantly downregulated in patients with DCM but not those with HCM (Fig. 2f), indicating that patients with HCM and DCM experienced various degrees of oxidative stress.

Previous studies have identified that the hypertrophic heart gradually switches the source of bioenergy metabolism from fatty acid oxidation to glycolysis[27,28]. To comprehensively detect the metabolites in glycolysis and precisely discriminate isomers, such as glucose-6-phosphate (G6P)–fructose 6-phosphate (F6P), we selected 39 patients with HCM that matched 8 non-HCM controls in age and measured the related metabolites using a derivatization method. We observed that metabolites in upper glycolysis, including glucose, G6P and F6P were significantly decreased, whereas metabolites in lower glycolysis, such as 3-phosphoglycerate (3PG) and phosphopyruvate (PEP), were significantly increased in patients with HCM (Fig. 2g). We detected most of tricarboxylic acid (TCA) cycle metabolites and observed that citrate and isocitrate were significantly elevated, whereas succinate levels were greatly reduced (>fivefold) in patients with HCM (Fig. 2g). Of note, most TCA cycle metabolites (such as *cis*-aconitic acid, isocitrate and succinate) were significantly decreased in patients with DCM compared to non-HCM controls (Extended Data Fig. 2d,e). Notably, the level of gluconate, a key metabolite in PPP, was dramatically increased in patients with HCM (>tenfold), suggesting that dysregulated amount of glucose entered into the PPP (Fig. 2g), whereas not significantly changed in patients with DCM (Extended Data Fig. 2d). Moreover, glucose may enter into amino sugar and nucleotide sugar metabolism pathway, evidenced by the increased levels of UDP-*N*-acetylglucosamine (UDP-GlcNAc) and UDP-galactose (UDP-Gal) (Fig. 2g). In addition, numerous purine and pyrimidine nucleotides, such as xanthosine 5-monophosphate (XMP), deoxyadenosine monophosphate (dAMP), uridine monophosphate (UMP) and cytidine monophosphate (CMP), were significantly increased (>1.5-fold) in patients with HCM (Fig. 2g). We further observed that aspartate showed >3.5-fold increases in abundance (Fig. 2g), consistent with the previous report that aspartate synthesis

Fig. 2 | Metabolomics perturbations in the heart tissues from patients with HCM. a, Volcano plot of metabolites detected by target metabolomics in HCM and non-HCM controls (ctrl). Significantly upregulated, downregulated (FDR $P<0.05$, fold change (FC) >1.5 or <0.67) and unchanged metabolites are colored in red, blue and gray, respectively. Top ten significantly increased or decreased metabolites of FC in each group are labeled. The horizontal line denotes FDR cutoff of 0.05 and the vertical lines denote a FC of 1.5 or 0.67. **b**, Relative intensity of carnitine related metabolites in ctrl ($n=16$), patients with HCM (n = 349) and patients with DCM ($n=46$). **c**, KEGG metabolic pathway enrichment of differential metabolites (FDR $P<0.05$, FC >1.5 or <0.67) between HCM and non-HCM controls. Fisher's exact test (one-side) followed by FDR-corrected *P* value was used and only pathways with FDR-corrected $P<0.05$ were presented. **d**,**e**, Relative intensity of metabolites involved in cysteine and methionine metabolism (**d**) and vitamin B6 metabolism (**e**) in ctrl ($n=16$) and HCM (n = 349). **f**, Relative intensity of metabolites involved in glutathione metabolism in ctrl ($n=16$), HCM ($n=349$) and patients with DCM ($n=46$). **g**, Schema of metabolic pathways with select metabolites. Relative intensity of glucose, G6P, F6P, F1,6P2, G3P, 3PG, 2PG and pyruvate were measured by a derivatization method. Color corresponds to the $\log_2$ FC between patients with HCM and non-HCM controls. Gray nodes represent metabolites that were not detected and borders are color-coded by statistical significance. GlcN-6P, *N*-acetyl-D-glucosamine 6-phosphate; UDP-GlcNAc, UDP-*N*-acetylglucosamine; G1P, glucose 1-phosphate; G3P, glyceraldehyde 3-phosphate; Thpp, thiamine pyrophosphate; PRPP, 5-phosphoribosyl diphosphate; AICAR, acadesine; IMP, inosine monophosphate; GMP, guanosine monophosphate; NAD, nicotinamide adenine dinucleotide; NAM, nicotinamide; NMN, nicotinamide mononucleotide. The box plots visualized as median and 25th and 75th percentiles, with whiskers indicating maximal and minimal values (**b**,**d**–**f**) (exact *P* values are provided in the source data). Statistical analyses were performed by two-sided Mann–Whitney *U*-test (**b**, **d**–**f**) and followed by Benjamini–Hochberg correction (**a**,**g**). Asterisks indicate significance as follows: NS, not significant, $P\geq0.05$, $^{*}P<0.05$, $^{**}P<0.01$, $^{***}P<0.001$, $^{****}P<0.0001$.

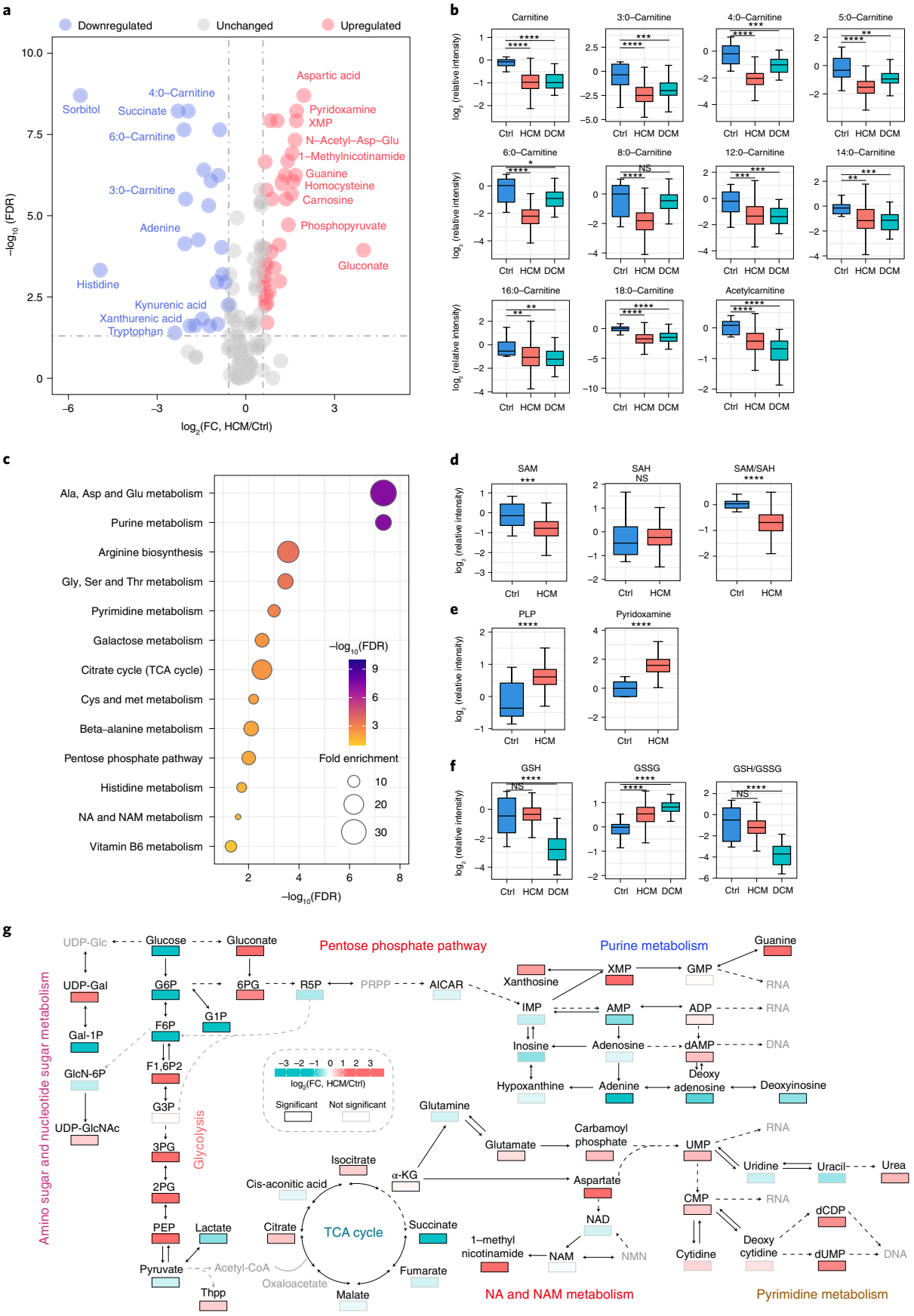
a
Downregulated
Unchanged
Upregulated
Sorbitol
Succinate
4:0–Carnitine
6:0–Carnitine
3:0–Carnitine
Adenine
Histidine
Kynurenic acid
Xanthurenic acid
Tryptophan
Aspartic acid
Pyridoxamine
XMP
N–Acetyl–Asp–Glu
1–Methylnicotinamide
Guanine
Homocysteine
Carnosine
Phosphopyruvate
Gluconate
−log10 (FDR)
log2(FC, HCM/Ctrl)
b
Carnitine
3:0–Carnitine
4:0–Carnitine
5:0–Carnitine
6:0–Carnitine
8:0–Carnitine
12:0–Carnitine
14:0–Carnitine
16:0–Carnitine
18:0–Carnitine
Acetylcarnitine
log2 (relative intensity)
Ctrl HCM DCM
c
Ala, Asp and Glu metabolism
Purine metabolism
Arginine biosynthesis
Gly, Ser and Thr metabolism
Pyrimidine metabolism
Galactose metabolism
Citrate cycle (TCA cycle)
Cys and met metabolism
Beta–alanine metabolism
Pentose phosphate pathway
Histidine metabolism
NA and NAM metabolism
Vitamin B6 metabolism
−log10(FDR)
Fold enrichment
d
SAM
SAH
SAM/SAH
e
PLP
Pyridoxamine
f
GSH
GSSG
GSH/GSSG
g
Amino sugar and nucleotide sugar metabolism
Glycolysis
Pentose phosphate pathway
Purine metabolism
TCA cycle
NA and NAM metabolism
Pyrimidine metabolism
UDP-Glc
Glucose
Gluconate
UDP-Gal
G6P
6PG
R5P
PRPP
AICAR
Gal-1P
G1P
F6P
GlcN-6P
F1,6P2
UDP-GlcNAc
G3P
3PG
2PG
PEP
Lactate
Pyruvate
Acetyl-CoA
Thpp
Citrate
Isocitrate
Cis-aconitic acid
α-KG
Succinate
Fumarate
Malate
Oxaloacetate
Glutamine
Glutamate
Carbamoyl phosphate
Aspartate
Xanthosine
XMP
GMP
Guanine
IMP
AMP
ADP
Inosine
Adenosine
dAMP
Hypoxanthine
Adenine
Deoxy adenosine
Deoxyinosine
RNA
DNA
UMP
Uridine
Uracil
Urea
CMP
Cytidine
Deoxy cytidine
dCDP
dUMP
NAD
NAM
NMN
1–methyl nicotinamide
Significant
Not significant

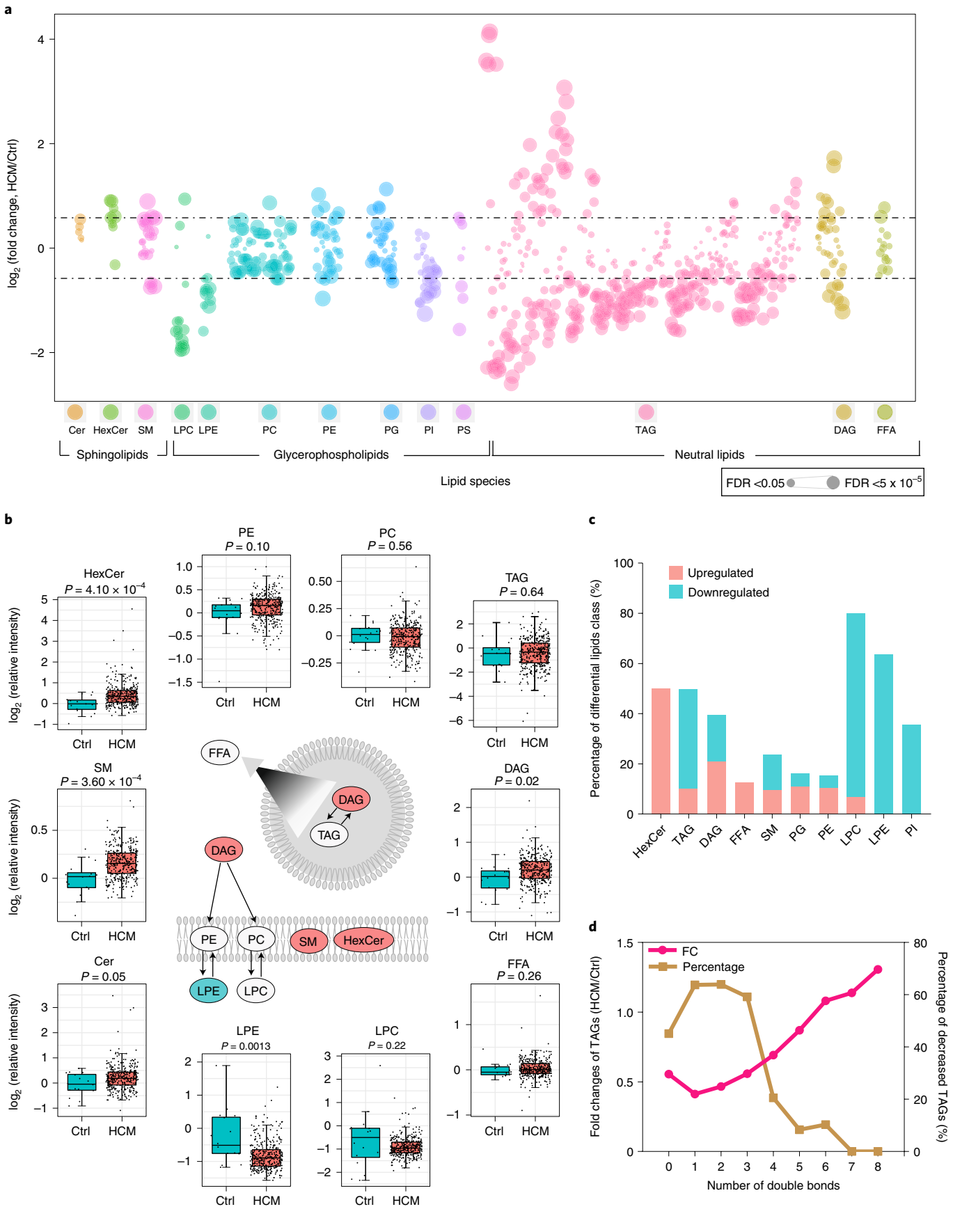
a
log2 (fold change, HCM/Ctrl)
Cer HexCer SM LPC LPE PC PE PG PI PS TAG DAG FFA
Sphingolipids
Glycerophospholipids
Neutral lipids
Lipid species
FDR <0.05
FDR <5 x 10−5
b
HexCer P = 4.10 × 10−4
PE P = 0.10
PC P = 0.56
TAG P = 0.64
SM P = 3.60 × 10−4
DAG P = 0.02
Cer P = 0.05
FFA P = 0.26
LPE P = 0.0013
LPC P = 0.22
log2 (relative intensity)
Ctrl HCM
FFA DAG TAG PE PC SM HexCer LPE LPC
c
Upregulated
Downregulated
Percentage of differential lipids class (%)
HexCer TAG DAG FFA SM PG PE LPC LPE PI
d
FC
Percentage
Fold changes of TAGs (HCM/Ctrl)
Percentage of decreased TAGs (%)
Number of double bonds

Fig. 3 | Lipidomics alterations in the heart tissues from patients with HCM. a, Bubble plot of log_2 FC in abundance of lipid species in HCM relative to non-HCM controls (ctrl). Values are shown as log_2 FC relative to non-HCM controls. Each dot represents a lipid species. Color-coded per lipid class. Dot size indicates significance. The horizontal lines denote FC of 1.5 or 0.67. **b**, Relative intensity of lipid classes in HCM ($n = 349$) and ctrl ($n = 16$). Illustration shows lipid classes that achieved statistically significant increase (red) and decrease (blue). The box plots are visualized as median and 25th and 75th percentiles, with whiskers indicating maximal and minimal values. **c**, The percentage of significantly upregulated (red) and downregulated (blue) (FDR-corrected $P < 0.05$, FC >1.5 or <0.67) lipid species for each lipid class. **d**, FC of TAGs and percentage of significantly decreased TAGs with different numbers of double bonds between HCM and non-HCM controls. Statistical analyses were performed by two-sided Mann–Whitney *U*-test (**b**) and followed by Benjamini–Hochberg correction (**a**,**c**).

is elevated to support biomass by enhancing glucose consumption during cardiac hypertrophy[29]. Taken together, these results suggest a dramatic and programmed change of metabolites in the heart of patients with HCM.

Strong correlations among metabolites may suggest that these metabolites share common functions and lie in related metabolic network[30]. To identify potential co-regulated relationships of the differential metabolites mentioned above, we performed correlation analysis and constructed correlation network for these metabolites. We discovered that 58% of differential metabolites displayed significant correlations with each other (Extended Data Fig. 2f). Of particular interest, we noticed that almost all the differential metabolites showed strong positive correlations (Extended Data Fig. 2g). As expected, metabolites in the same metabolic pathway (such as carnitine synthesis) showed a strong correlation (Extended Data Fig. 2g). Succinate, which acts as an electron carrier in the mitochondrial electron transport chain[31], showed a significant positive correlation with multiple carnitines (Extended Data Fig. 2f,g), suggesting the mutual regulation between fatty acid oxidation and succinate[22]. Collectively, our findings highlight that the metabolic alterations are highly coordinated in patients with HCM.

Lipidomic alterations in the heart tissues from patients with HCM. Given the essential roles of lipids, such as ceramides and triacylglycerols (TAGs), in underlying the pathogenesis and predicting the risk of cardiovascular diseases[32,33], we further conducted lipidomics analysis to characterize the lipid profile of patients with HCM. Partial least squares discrimination analysis (PLS-DA) showed that patients with HCM had a distinct lipid profile compared to non-HCM controls (Extended Data Fig. 3a). All the detected lipids were showed in a bubble plot according to lipid classes, with 301 differential lipids (73 upregulated and 228 downregulated) between patients with HCM and non-HCM controls (Fig. 3a). Of note, the subclasses of sphingolipids including hexosylceramide (HexCer) and sphingomyelin (SM) were significantly upregulated in patients with HCM (Fig. 3b); 50% of detected individual sphingolipids were significantly increased in patients with HCM (Extended Data Fig. 3b). Given that previous study has demonstrated the de novo synthesis of sphingolipids as a requirement for pathogenesis of lipotoxic cardiomyopathy and hypertrophy[34], our data suggest that intervening with sphingolipids metabolism might serve as a potential target for HCM treatment. Glycerophospholipids, including lysophosphatidylethanolamine (LPE) and phosphatidylinositol (PI), were significantly reduced and most of detected individual LPE and lysophosphatidylcholine (LPC) were significantly decreased in patients with HCM (Fig. 3b,c and Extended Data Fig. 3c,e), indicating the cytosolic phospholipase A_2 (PLA_2), an enzyme that generates fatty acids and lysophospholipids from phospholipids, was dysregulated in patients with HCM. A previous study has reported that PLA_2 deficiency induces hypertrophy growth of heart and exaggerates pathologic stress-induced cardiac hypertrophy[35]. The remaining glycerophospholipids, including phosphatidylethanolamine (PE), phosphatidylcholine (PC) and phosphatidylglycerol (PG), showed no difference between patients with HCM and non-HCM controls (Fig. 3b and Extended Data Fig. 3e). Nevertheless, individual lipids in PE, PC and PG, such as PE34:3(16:1/18:2), PC36:3(18:0/18:3) and PG36:3(18:0/18:3), were significantly upregulated in patients with HCM (Extended Data Fig. 3c). Among neutral lipids, diacylglycerol (DAG) class was significantly increased with no change of TAG and free fatty acid (FFA) (Fig. 3b), whereas 40% detected individual TAGs were significantly decreased in patients with HCM (Fig. 3c and Extended Data Fig. 3d). A closer examination of fatty acid composition of TAGs revealed that the TAGs containing lower double-bond content showed a more obvious downregulation in patients with HCM (Fig. 3d). Moreover, the proportion of significantly downregulated TAGs was elevated with the decrease of double-bond content in patients with HCM (Fig. 3d), whereas TAGs showed no constant changing trend along with their carbon number (Extended Data Fig. 3f). Taken together, lipidomics data indicate significant alterations of complex lipids between patients with HCM and non-HCM controls.

Metabolic disturbances in plasma from patients with HCM. To further determine the plasma metabolic perturbations and compare the metabolic alteration between the plasma and cardiac tissues from patients with HCM, we profiled the plasma samples from non-HCM controls and patients with HCM by using metabolomics analyses. A clear segregation between patients with HCM and non-HCM controls was observed (Extended Data Fig. 4a,b). We totally identified 34 differential metabolites (22 upregulated and 12 downregulated) in the circulating plasma between patients with HCM and non-HCM controls (Fig. 4a). Comparing the metabolic alteration in the plasma

Fig. 4 | Metabolic disturbances in plasma samples from patients with HCM. a, Volcano plot of metabolites detected by target metabolomics in the plasma of HCM and non-HCM controls (ctrl). Significantly upregulated, downregulated (FDR-corrected $P < 0.05$, FC >1.5 or <0.67) and unchanged metabolites are colored in purple, orange and gray, respectively. Top ten significantly increased or decreased metabolites of FC in each group are labeled. The horizontal line denotes a FDR cutoff of 0.05 and the vertical lines denote a FC of 1.5 or 0.67. **b**, Log_2 FC of common metabolites in the tissue (*x* axis) and plasma (y axis) of patients with HCM compared to non-HCM controls. Differential metabolites with opposite or consistent alteration were marked with different colors. **c**, KEGG metabolic pathway enrichment of differential metabolites between HCM and non-HCM controls in plasma and heart tissue. Fisher's exact test (one-sided) followed by FDR-corrected *P* value was used and only pathways with FDR-corrected $P < 0.05$ were presented, mean absolute (abs.) log_2 FC of metabolites enriched in each pathway was calculated. **d**, Log_2 FC of significantly changed metabolites in glutathione metabolism, purine metabolism, glucose-related metabolism pathway and carnitine synthesis pathway in plasma or heart tissue of patients with HCM. **e**, Schematic of the dataset creation and analysis strategy for the diagnosis of HCM. C, non-HCM controls; H, HCM. **f**,**g**, Receiver operating characteristic (ROC) curve (**f**) and precision-recall curve (PRC) (**g**) of the random forest model in the testing set. Statistical analyses were performed by two-sided Mann–Whitney *U*-test and followed by Benjamini–Hochberg correction (**a**,**d**).

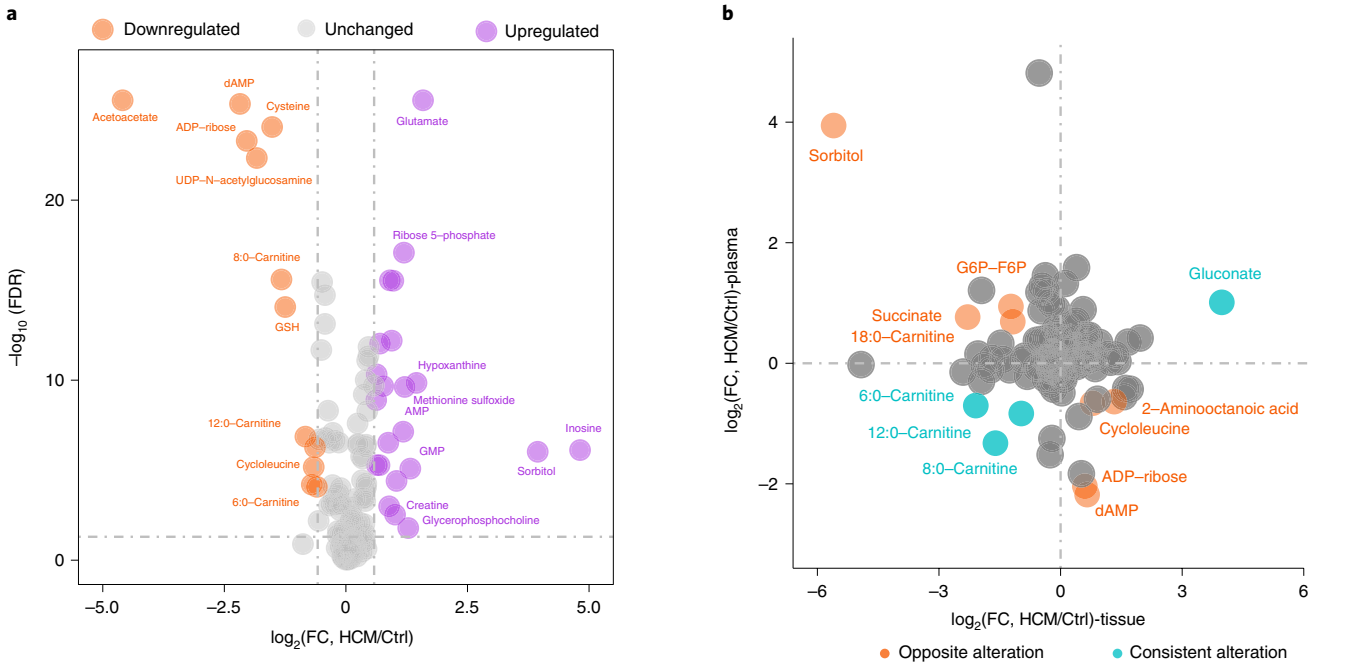
a
Downregulated
Unchanged
Upregulated
Acetoacetate
dAMP
Cysteine
ADP–ribose
UDP–N–acetylglucosamine
Glutamate
Ribose 5–phosphate
8:0–Carnitine
GSH
Hypoxanthine
Methionine sulfoxide
AMP
12:0–Carnitine
Inosine
GMP
Cycloleucine
Sorbitol
6:0–Carnitine
Creatine
Glycerophosphocholine
−log10 (FDR)
log2(FC, HCM/Ctrl)
b
Sorbitol
G6P–F6P
Gluconate
Succinate
18:0–Carnitine
6:0–Carnitine
2–Aminooctanoic acid
Cycloleucine
12:0–Carnitine
8:0–Carnitine
ADP–ribose
dAMP
log2(FC, HCM/Ctrl)-plasma
log2(FC, HCM/Ctrl)-tissue
Opposite alteration
Consistent alteration

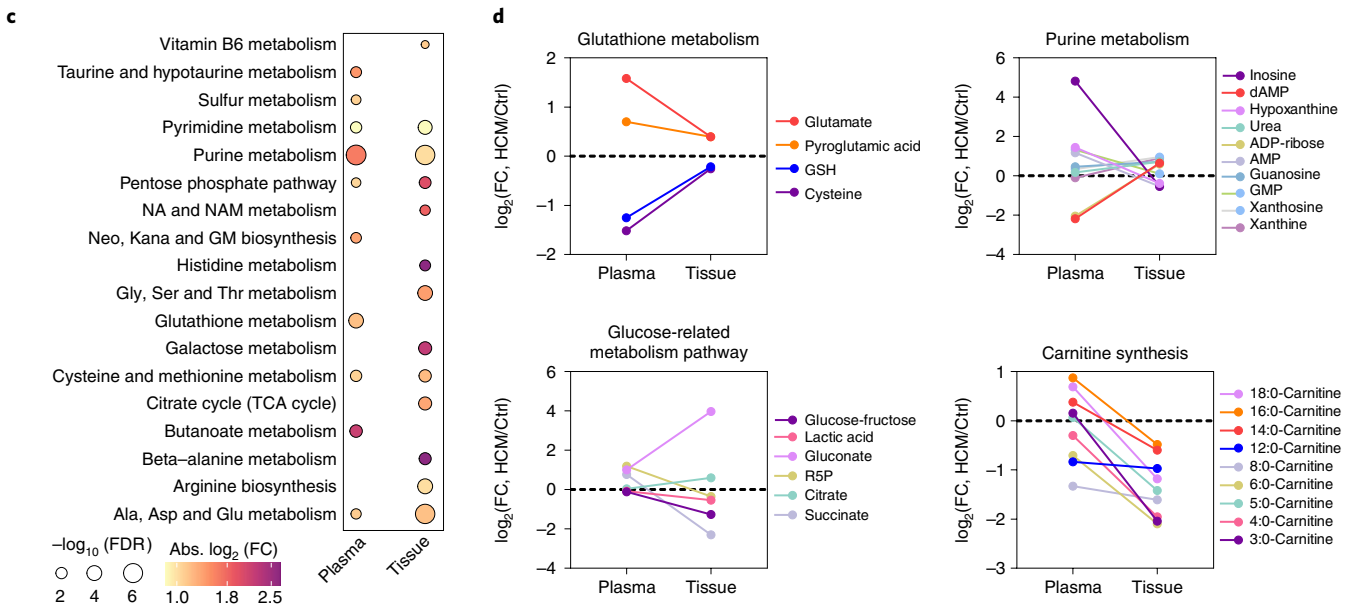
c
Vitamin B6 metabolism
Taurine and hypotaurine metabolism
Sulfur metabolism
Pyrimidine metabolism
Purine metabolism
Pentose phosphate pathway
NA and NAM metabolism
Neo, Kana and GM biosynthesis
Histidine metabolism
Gly, Ser and Thr metabolism
Glutathione metabolism
Galactose metabolism
Cysteine and methionine metabolism
Citrate cycle (TCA cycle)
Butanoate metabolism
Beta–alanine metabolism
Arginine biosynthesis
Ala, Asp and Glu metabolism
−log10 (FDR)
Abs. log2 (FC)
Plasma
Tissue
d
Glutathione metabolism
Glutamate
Pyroglutamic acid
GSH
Cysteine
Purine metabolism
Inosine
dAMP
Hypoxanthine
Urea
ADP-ribose
AMP
Guanosine
GMP
Xanthosine
Xanthine
Glucose-related metabolism pathway
Glucose-fructose
Lactic acid
Gluconate
R5P
Citrate
Succinate
Carnitine synthesis
18:0-Carnitine
16:0-Carnitine
14:0-Carnitine
12:0-Carnitine
8:0-Carnitine
6:0-Carnitine
5:0-Carnitine
4:0-Carnitine
3:0-Carnitine
log2(FC, HCM/Ctrl)

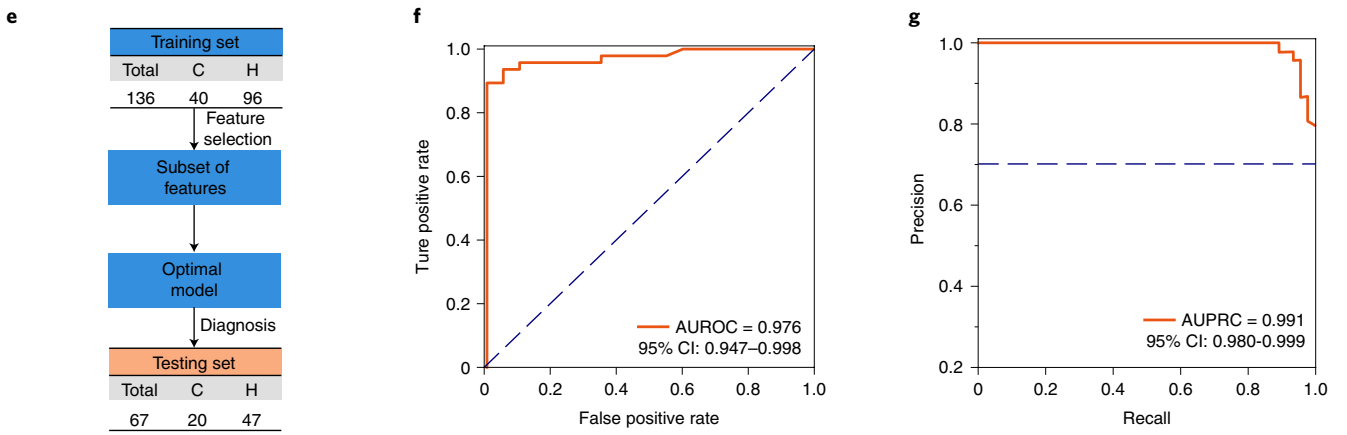
e
Training set
Total C H
136 40 96
Feature selection
Subset of features
Optimal model
Diagnosis
Testing set
Total C H
67 20 47
f
Ture positive rate
False positive rate
AUROC = 0.976
95% CI: 0.947–0.998
g
Precision
Recall
AUPRC = 0.991
95% CI: 0.980-0.999

and cardiac tissues from patients with HCM, we observed that there were 12 common differential metabolites in the plasma and cardiac tissues (Extended Data Fig. 4c) and most of them exhibited opposite alteration trend in these two types of samples (Fig. 4b). To compare the differences in dysregulated metabolic pathways between plasma and cardiac tissues of patients with HCM, we performed pathway enrichment analysis individually for the differential metabolites in these two types of samples, respectively. We observed that purine and pyrimidine metabolism pathway were significantly perturbated in both plasma and cardiac tissues, whereas glutathione metabolism pathway and related metabolites were only significantly perturbated in plasma (Fig. 4c,d). Specifically, most of the metabolites in purine metabolism pathway displayed opposite alteration trend in the plasma and cardiac tissues of patients with HCM (Fig. 4d). Most of metabolites in glucose-related metabolism pathway (glycolysis, PPP and TCA cycle) significantly altered only in the cardiac tissues of patients with HCM (Fig. 4d). Of note, short-chain carnitines (for example, 6:0-Carnitine, 5:0-Carnitine and 3:0-Carnitine) were significantly decreased both in the plasma and cardiac tissues of patients with HCM (Fig. 4d). Conversely, long-chain carnitines (18:0-Carnitine and 14:0-Carnitine) were significantly downregulated in the cardiac tissues, but significantly upregulated in the plasma (Fig. 4d).

To identify diagnostic biomarkers for distinguishing non-HCM controls and patients with HCM, we performed feature selection with 142 metabolites in plasma and used the selected features to build a random forests classifier on the training dataset. We then ran the established classifier in testing dataset to measure the independent performance of our model (Fig. 4e). The random forests model by a biomarker panel of five metabolites (8:0-carnitine, hypoxanthine, creatine, phenylalanine and tryptophan) enabled the discrimination between non-HCM and HCM groups with area under the receiver operating characteristic curve of 0.976 (0.947–0.998) and area under the precision-recall curve of 0.991 (0.98–0.999) (Fig. 4f,g). Collectively, these findings reveal the differences of metabolic alteration between plasma and cardiac tissues of patients with HCM and demonstrate the power of metabolomics for biomarker discovery, which may make the diagnosis of HCM more accessible.

Metabolic association with the genotypes and cardiac function in patients with HCM. Numerous mutations within genes encoding sarcomeric proteins cause remarkable genetic heterogeneity of HCM[6,7]. To gain better insight into HCM pathogenesis, we determined the metabolic profiles of patients with HCM with different genotypes. PCA showed that similar metabolic profiles were observed between patients with or without gene mutations and among patients with diverse pathogenic genes (Fig. 5a,b). Notably, there was no differential metabolite ($P<0.05$, fold change >1.25 or <0.8) between patients with *MYH7* ($n=98$) and *MYBPC3* ($n=67$) mutations, the two most common pathogenic genes (Fig. 5c). Thus, these data suggest that myocardial metabolism is not clearly affected by genetic heterogeneity in patients with HCM.

The NYHA class is regarded as an indicator of cardiac function for patients with HCM and higher NYHA class indicates worse cardiac function[12,36]. Odd ratios (ORs) of NYHA class were estimated by using univariate and multivariate logistic regression analyses to determine the correlation between metabolites and NYHA class. Univariate analysis revealed that galactose 1-phosphate and UDP-Gal, the metabolites in galactose metabolism, were positively and inversely associated with NYHA class, respectively (Fig. 5d). Notably, almost all the purine and pyrimidine metabolism related metabolites were significantly related to higher NYHA class, indicating that excess biomass supplementation may lead to worse cardiac function of HCM (Fig. 5d). Of note, metabolites in glucose-related metabolic pathways, including glycolysis and PPP, also exhibited significantly positive associations with NYHA class (Fig. 5d). In addition, medium- and long-chain carnitines were inversely associated with NYHA class (Fig. 5d). Of note, significant correlations with increased NYHA class were observed for most TAGs (Fig. 5e). Multivariate analysis indicated that galactose 1-phosphate, UDP-Gal, G6P-F6P and GSSG were major factors that associated with NYHA class (Fig. 5f). Taken together, these findings showed significant correlation of the level of metabolites with the cardiac function, suggesting a potential role of metabolic profiling for the evaluation of cardiac function.

Metabolic subtyping of the heart tissues from patients with HCM. Given the lack of effective molecular typing in HCM[12,36], we evaluated whether metabolic profiles could be harnessed for molecularly subtyping patients with HCM. Consensus clustering based on metabolomics data identified three subgroups with distinct metabolic profiles (Fig. 6a,b and Extended Data Fig. 5a–d). We then examined the survival outcomes among the three subtypes patients, which revealed a clear separation between subtype I (S-I) and S-II or S-III ($P=0.25$, log-rank test) (Fig. 6c). Moreover, patients with NYHA class I and II were more prominent in S-I over other two subtypes ($P=2.8\times10^{-8}$, two-sided Fisher's exact test), whereas maximum left ventricular wall thickness (MWT) ($P=0.34$) showed no significant difference among the three subtypes (Extended Data Fig. 5e,f).

To further investigate the metabolic differences in each distinct subtype, we performed KEGG pathway enrichment analyses and observed that glutathione metabolism and TCA cycle were only significantly enriched between S-I and S-II and S-I and S-III (Fig. 6d). Notably, the differential metabolites (FDR-corrected $P<0.05$, fold change >1.25 or <0.8), involved in glutathione metabolism and TCA cycle, displayed consistent upward or downward trend among different subtypes (Fig. 6e). Consistently, patients with higher levels of TCA cycle metabolites (isocitrate and fumarate) had better survival outcomes, suggesting an energetic compensation may eventually impose beneficial effects on patient outcomes[37,38] (Extended Data Fig. 5g). In addition, purine metabolism was identified as the most significantly changed pathway among the three subtypes and most of the purine and pyrimidine metabolism related metabolites were increased in S-II and S-III compared to S-I (Fig. 6e). Moreover, patients with high levels of purine and pyrimidine related metabolites exhibited poor survival outcomes (Extended Data Fig. 5h). Of note, medium- and long-chain carnitines were significantly downregulated in S-II and S-III. On the contrary, short-chain carnitines were significantly upregulated in S-II and S-III (Fig. 6e).

Fig. 5 | Metabolic association with clinical characteristics in patients with HCM. a, PCA score plot of metabolomics and lipidomics data on patients with HCM with or without gene mutations. **b**, PCA score plot of metabolomics and lipidomics data on patients with HCM with different pathogenic genes. **c**, Volcano plot of metabolites alterations between patients with HCM with *MYBPC3* ($n=67$) and *MYH7* (n = 98). Unchanged metabolites were colored in gray. The horizontal line denotes *P* value cutoff of 0.05 and the vertical lines denote FC of 1.25 or 0.8. Statistical analyses were performed by two-sided Mann–Whitney *U*-test. **d**, Forest plot of ORs for the association between NYHA class and the relative abundance of metabolites detected by targeted metabolomics. Metabolites in different metabolic pathways were marked with different colors. OR were presented by the center of error bars and 95% confidence intervals were presented by the line widths. **e**, Forest plot of OR for the association between NYHA class and the relative abundance of TAGs, the abundance of TAGs was defined as the ratio of each TAG to total TAG abundance in each patient. ORs are presented by the center of error bars and 95% confidence intervals are presented by the line widths. **f**, OR and 95% confidence intervals for the association between NYHA class and metabolites based on multivariate logistic regression analysis. ORs are presented by the center of error bars and 95% confidence intervals are presented by the line widths.

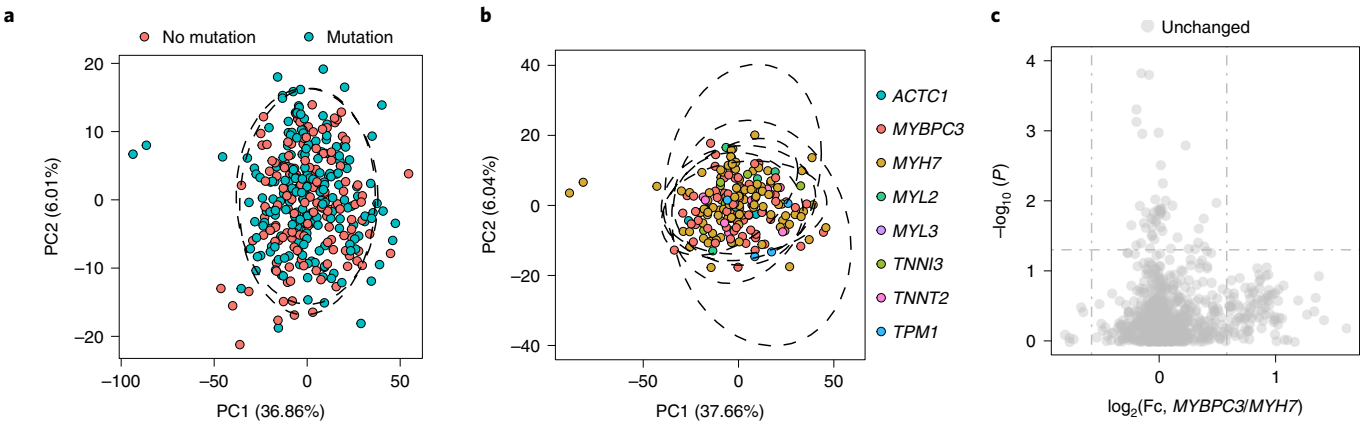
a
No mutation
Mutation
PC2 (6.01%)
PC1 (36.86%)
b
PC2 (6.04%)
PC1 (37.66%)
ACTC1
MYBPC3
MYH7
MYL2
MYL3
TNNI3
TNNT2
TPM1
c
Unchanged
−log10 (P)
log2(Fc, MYBPC3/MYH7)

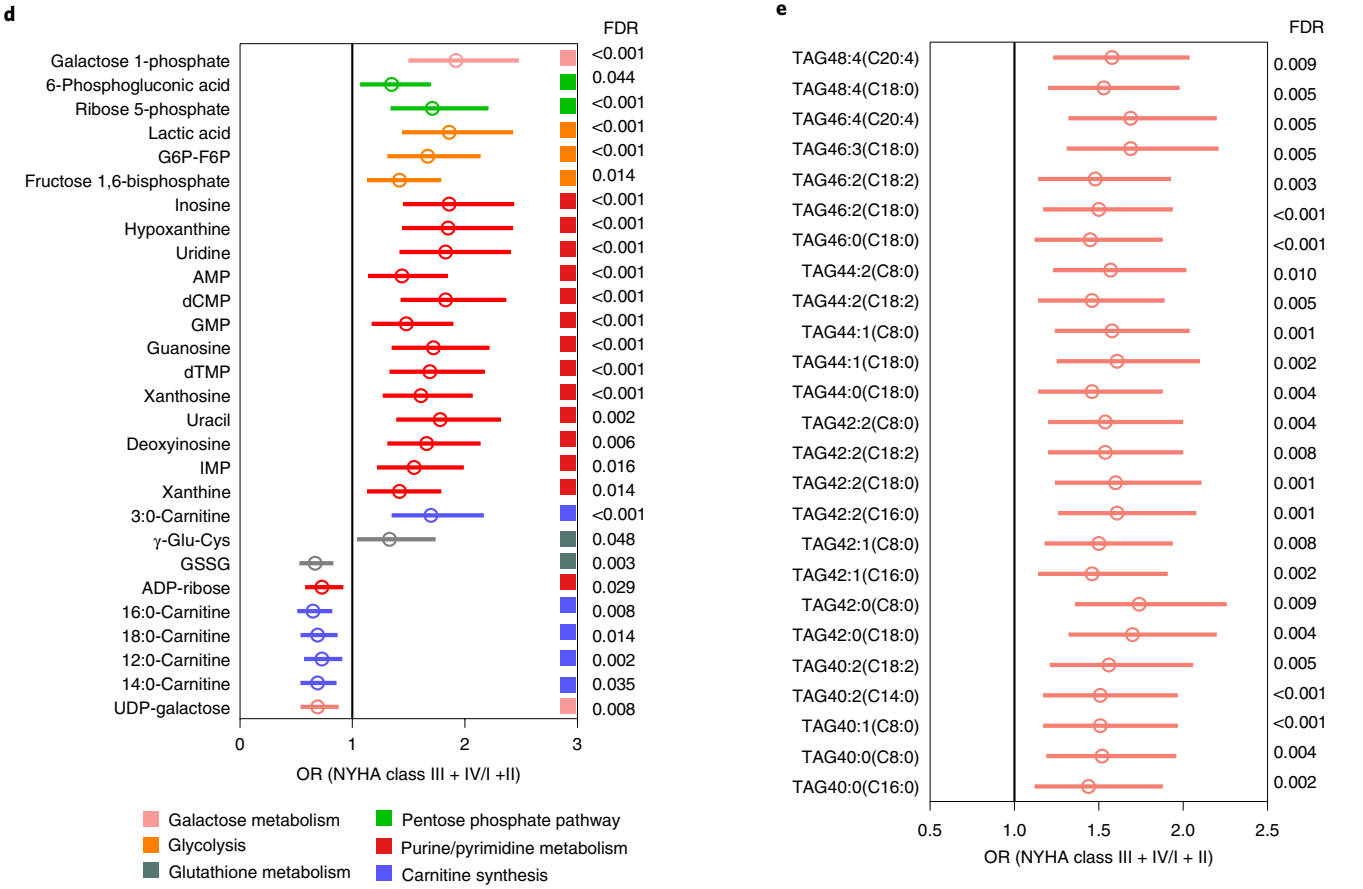
d
FDR
Galactose 1-phosphate <0.001
6-Phosphogluconic acid 0.044
Ribose 5-phosphate <0.001
Lactic acid <0.001
G6P-F6P <0.001
Fructose 1,6-bisphosphate 0.014
Inosine <0.001
Hypoxanthine <0.001
Uridine <0.001
AMP <0.001
dCMP <0.001
GMP <0.001
Guanosine <0.001
dTMP <0.001
Xanthosine <0.001
Uracil 0.002
Deoxyinosine 0.006
IMP 0.016
Xanthine 0.014
3:0-Carnitine <0.001
γ-Glu-Cys 0.048
GSSG 0.003
ADP-ribose 0.029
16:0-Carnitine 0.008
18:0-Carnitine 0.014
12:0-Carnitine 0.002
14:0-Carnitine 0.035
UDP-galactose 0.008
OR (NYHA class III + IV/I +II)
Galactose metabolism
Glycolysis
Glutathione metabolism
Pentose phosphate pathway
Purine/pyrimidine metabolism
Carnitine synthesis
e
FDR
TAG48:4(C20:4) 0.009
TAG48:4(C18:0) 0.005
TAG46:4(C20:4) 0.005
TAG46:3(C18:0) 0.005
TAG46:2(C18:2) 0.003
TAG46:2(C18:0) <0.001
TAG46:0(C18:0) <0.001
TAG44:2(C8:0) 0.010
TAG44:2(C18:2) 0.005
TAG44:1(C8:0) 0.001
TAG44:1(C18:0) 0.002
TAG44:0(C18:0) 0.004
TAG42:2(C8:0) 0.004
TAG42:2(C18:2) 0.008
TAG42:2(C18:0) 0.001
TAG42:2(C16:0) 0.001
TAG42:1(C8:0) 0.008
TAG42:1(C16:0) 0.002
TAG42:0(C8:0) 0.009
TAG42:0(C18:0) 0.004
TAG40:2(C18:2) 0.005
TAG40:2(C14:0) <0.001
TAG40:1(C8:0) <0.001
TAG40:0(C8:0) 0.004
TAG40:0(C16:0) 0.002
OR (NYHA class III + IV/I + II)

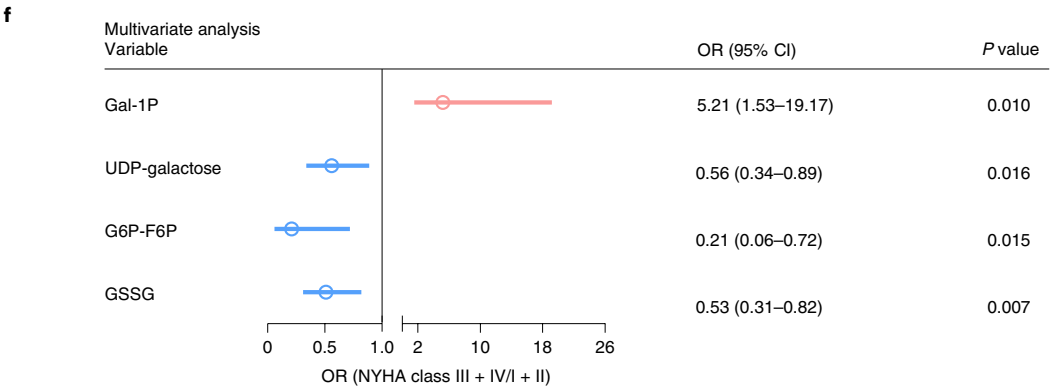
f
Multivariate analysis
Variable
OR (95% CI)
P value
Gal-1P 5.21 (1.53–19.17) 0.010
UDP-galactose 0.56 (0.34–0.89) 0.016
G6P-F6P 0.21 (0.06–0.72) 0.015
GSSG 0.53 (0.31–0.82) 0.007
OR (NYHA class III + IV/I + II)

Consensus clustering analysis on lipidomics data also identified three subgroups (Fig. 6f and Extended Data Fig. 5i–l). The distribution of patients with different NYHA class ($P=0.99$) had no significant difference among the three subtypes (Extended Data Fig. 5m). However, MWT ($P=0.016$) and survival outcomes ($P=0.0084$) were significantly differed among the three subtypes (Fig. 6g and Extended Data Fig. 5n) and patients in S-I had the best clinical prognosis, whereas patients in S-II had the poorest prognosis ($P=0.004$) (Fig. 6g). Comparing the differential metabolites between S-I and S-II, we found that most of differential metabolites belong to TAGs. Notably, the proportion of TAGs with low carbon number (<54) were significantly increased in S-II, whereas those with high carbon number (≥54) were significantly increased in S-I (Fig. 6h). Consistently, we found that the high proportion of TAGs with low carbon number (<54) accompanied with poor survival outcomes, whereas the low proportion of TAGs with high carbon number (≥54) accompanied with poor survival outcomes (Extended Data Fig. 5o). TAGs with longer chains may produce more long-chain fatty acids, which enhances energy supply for cardiomyocytes[39] and maintains normal cytosolic Ca^{2+} cycling[40], which are beneficial for improving the pathological and clinical features of HCM[9]. Notably, the level of HexCer d18:1/22:2, a hexosylceramide, was significantly elevated in patients with HCM and patients with high level of HexCer d18:1/22:2 presented poor survival outcomes (Extended Data Figs. 3b and 5p). Taken together, our results indicate that HCM are molecularly diversified, which may benefit the potential personalized therapies of patients with HCM.

Survival outcomes of patients with HCM predicted by machine learning. To determine whether a panel of metabolites could be identified to predict the survival outcomes for patients with HCM, we performed the feature selection with all the 922 detected metabolites and built a prediction model by using random survival forests on the training dataset. Then, we applied the model to predict the survival outcomes in testing dataset to measure the performance of our model (Fig. 6i). Finally, we selected a panel of 12 metabolites (including dimethylglycine, *N*-acetyl-L-glutamine, γ-aminobutyric acid, XMP, 18:0-Carnitine, GMP, UDP-galactose, PC38:6p(16:0/22:6), PE32:0(16:0/16:0), PS34:3(16:1/18:2), PG38:6(18:2/20:4) and TAG52:2(C18:0)), which showed remarkable predictive power (C-index, 0.916 (0.814–0.978)) for predicting the survival outcomes of patients with HCM (Fig. 6j). Thus, our findings identify a potential metabolite panel as prognostic predictor for HCM.

Metabolomics and proteomics analyses reveal potential therapeutic strategies for HCM. Given that proteomics analysis can provide an orthogonal perspective of metabolism by profiling the metabolic proteins and thereby facilitate the understanding HCM metabolism, we thus conducted a global proteomics study on patients with HCM and non-HCM control samples. In total, 643 proteins were identified as differential between the two groups (FDR-corrected $P<0.05$), with 403 upregulated and 240 downregulated in patients with HCM from 3,737 quantified proteins. Notably, KEGG pathway enrichment analysis of differential proteins revealed that multiple metabolic pathways, such as oxidative phosphorylation, PPP and glycolysis, were significantly altered in patients with HCM (Fig. 7a). Of note, oxidative phosphorylation was identified as the most significantly changed metabolism pathway with decrease in substantial subunits of mitochondrial respiration chain complexes, suggesting a dramatic downregulation of ATP generation in patients with HCM (Fig. 7b).

Combining metabolomics and proteomics datasets, we found that PPP was altered both in metabolite and protein levels (Figs. 2c and 7a). PPP produces precursors for nucleotide biosynthesis by using the glycolysis intermediates[41]. Moreover, our study revealed that purine and pyrimidine metabolism pathways were significantly altered in patients with HCM (Fig. 2c) and the related metabolites were highly correlated with NYHA class and survival outcomes (Fig. 5d and Extended Data Fig. 5h). Therefore, it is reasonable to speculate that the upregulation of PPP may result in the increase of purine and pyrimidine metabolism related metabolites and thus support the expansion of biomass, ultimately leading to pathogenesis of cardiac hypertrophy. This prompted us to further explore the roles of PPP and purine and pyrimidine metabolism by integrating the metabolomics and proteomics data. We observed that the rate-limiting enzyme of PPP, glucose-6-phosphate dehydrogenase (G6PD), was increased in patients with HCM (>1.2-fold), although not significantly, in agreement with the decreased G6P and increased 6-phosphpogluconate (6PG) (Fig. 7c). To validate the proteomics data, we performed western blotting and observed the significantly increased protein levels of G6PD in patients with HCM (Fig. 7c). In addition, PPP is a major source generating nicotinamide adenine dinucleotide phosphate (NADPH), which plays a crucial role in the maintenance of cellular redox status[41]. Previous studies have demonstrated that oxidative stress is enhanced in HCM[42] and the antioxidant glutathione precursor *N*-acetylcysteine effectively reversed myocyte hypertrophy, interstitial fibrosis and cardiac function in animal models of HCM[25,26]. Consistent with these reports, our data indicated that hearts in patients with HCM may experience higher oxidative stress and the subsequential redox imbalance. It can be proposed that to maintain the redox homeostasis, the expression of G6PD in the hearts of patients with HCM was upregulated to produce more NADPH thereby enhance their capacity for regenerating GSH. In addition, the mitochondrial activities were downregulated, evidenced by the overall downregulation of mitochondrial respiration chain complexes and the dramatic reduction of succinate, to reduce the reactive oxygen species generation as a compensation (Fig. 7d). Together, our metabolomics and proteomics data highlight that intervening with the PPP and oxidative stress might serve as potential therapeutic targets for HCM.

Fig. 6 | Metabolic subtyping and prognostic prediction of patients with HCM. a, Consensus clustering analysis based on metabolomics data of patients with HCM identified three subtypes. **b**, Heat map of metabolites relative abundance in each individual metabolic subtype. **c**, Kaplan–Meier curves for overall survival of patients with HCM among the three subtypes (Log-rank test). **d**, KEGG metabolic pathways enriched by significantly changed metabolites (two-side Kruskal–Wallis tests, FDR-corrected $P<0.05$, FC >1.25 or <0.8) in each individual metabolic subtype. Fisher's exact test (one-sided) followed by FDR-corrected *P* value was used. Only pathways with FDR-corrected $P<0.05$ were presented. Mean absolute (abs.) $\log_2$ FC of metabolites enriched in each pathway was calculated. **e**, Relative intensity of significantly changed metabolites between S-II or S-III and S-I in glutathione metabolism, TCA cycle, purine and pyrimidine metabolism and carnitine synthesis pathway. Data were presented as mean ± sd. **f**, Consensus clustering analysis based on lipidomics data of patients with HCM identified three subtypes. **g**, Kaplan–Meier curves for overall survival of patients with HCM among three subtypes (pairwise log-rank test). **h**, Bubble plot of $\log_2$ FC in abundance of significantly changed TAGs (Kruskal–Wallis test, FDR-corrected $P<0.05$, FC >1.25 or <0.8) in S-II relative to S-I. Each dot represents a TAG species. Color-coded per number of TAGs carbon. Dot size indicates significance. The horizontal lines denote FC of 1.25 or 0.8. The abundance of TAGs was defined as the ratio of each TAG to total TAG abundance in each patient. **i**, Schematic of the dataset creation and analysis strategy for the prediction of survival outcomes. S, survived; D, deceased. **j**, C-index values of the level of metabolites for overall survival in the testing dataset. Error bars represent 95% confidence intervals.

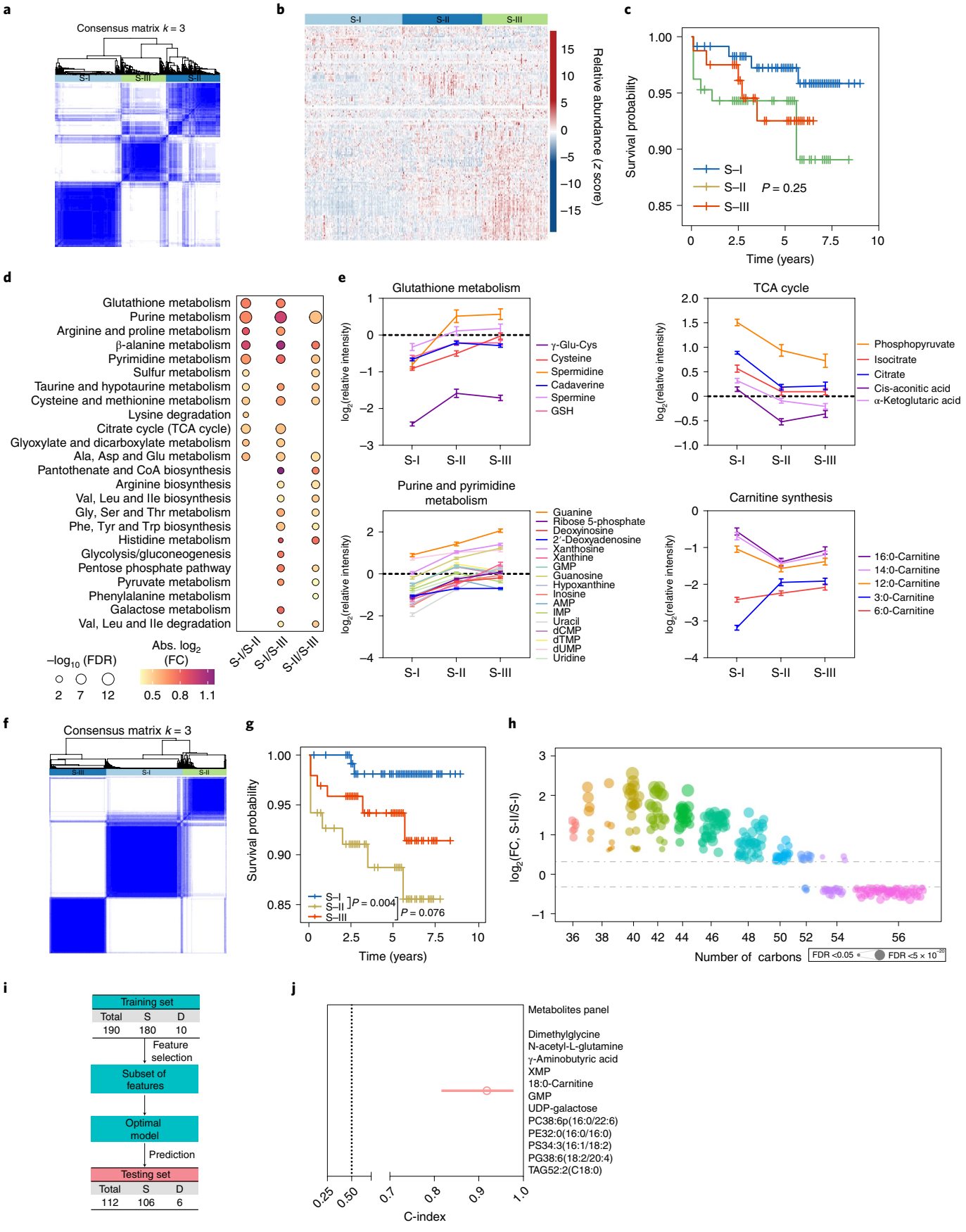
a
Consensus matrix k = 3
S-I
S-III
S-II
b
S-I
S-II
S-III
15
10
5
0
−5
−10
−15
Relative abundance (z score)
c
Survival probability
1.00
0.95
0.90
0.85
S–I
S–II
S–III
P = 0.25
0
2.5
5
7.5
10
Time (years)
d
Glutathione metabolism
Purine metabolism
Arginine and proline metabolism
β-alanine metabolism
Pyrimidine metabolism
Sulfur metabolism
Taurine and hypotaurine metabolism
Cysteine and methionine metabolism
Lysine degradation
Citrate cycle (TCA cycle)
Glyoxylate and dicarboxylate metabolism
Ala, Asp and Glu metabolism
Pantothenate and CoA biosynthesis
Arginine biosynthesis
Val, Leu and Ile biosynthesis
Gly, Ser and Thr metabolism
Phe, Tyr and Trp biosynthesis
Histidine metabolism
Glycolysis/gluconeogenesis
Pentose phosphate pathway
Pyruvate metabolism
Phenylalanine metabolism
Galactose metabolism
Val, Leu and Ile degradation
S-I/S-II
S-I/S-III
S-II/S-III
−log10 (FDR)
2 7 12
Abs. log2 (FC)
0.5 0.8 1.1
e
Glutathione metabolism
log2(relative intensity)
γ-Glu-Cys
Cysteine
Spermidine
Cadaverine
Spermine
GSH
TCA cycle
Phosphopyruvate
Isocitrate
Citrate
Cis-aconitic acid
α-Ketoglutaric acid
Purine and pyrimidine metabolism
Guanine
Ribose 5-phosphate
Deoxyinosine
2′-Deoxyadenosine
Xanthosine
Xanthine
GMP
Guanosine
Hypoxanthine
Inosine
AMP
IMP
Uracil
dCMP
dTMP
dUMP
Uridine
Carnitine synthesis
16:0-Carnitine
14:0-Carnitine
12:0-Carnitine
3:0-Carnitine
6:0-Carnitine
S-I
S-II
S-III
f
Consensus matrix k = 3
S-III
S-I
S-II
g
Survival probability
S–I
S–II
S–III
P = 0.004
P = 0.076
Time (years)
h
log2(FC, S-II/S-I)
Number of carbons
FDR <0.05
FDR <5 × 10−20
i
Training set
Total S D
190 180 10
Feature selection
Subset of features
Optimal model
Prediction
Testing set
Total S D
112 106 6
j
Metabolites panel
Dimethylglycine
N-acetyl-L-glutamine
γ-Aminobutyric acid
XMP
18:0-Carnitine
GMP
UDP-galactose
PC38:6p(16:0/22:6)
PE32:0(16:0/16:0)
PS34:3(16:1/18:2)
PG38:6(18:2/20:4)
TAG52:2(C18:0)
C-index

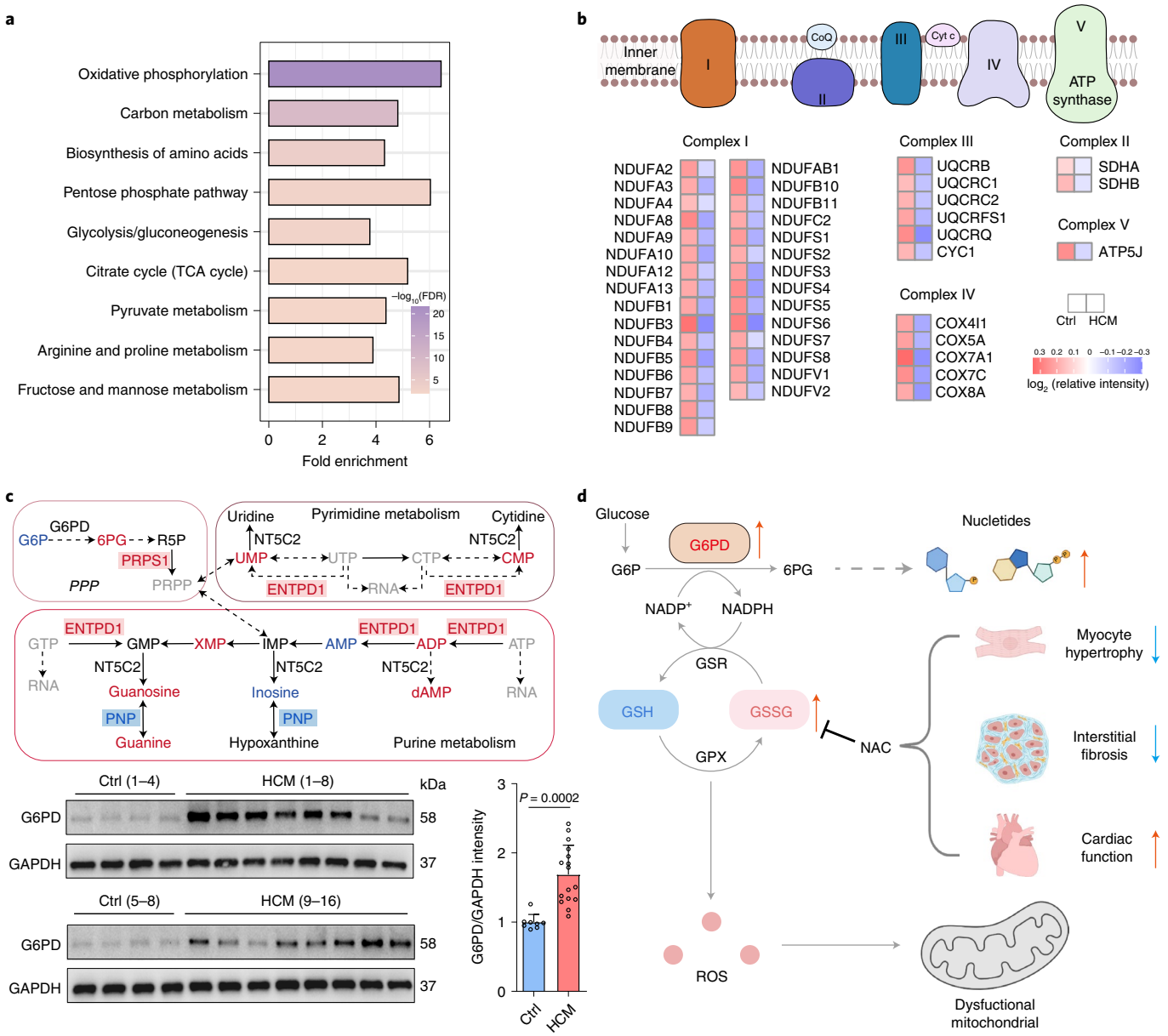

Fig. 7 | Metabolomics and proteomics analyses reveal potential therapeutic strategies for HCM. a, KEGG pathways enriched by significantly changed proteins (FDR-corrected $P < 0.05$) in patients with HCM. Fisher's exact test (one-sided) followed by FDR-corrected P value was used. Only pathways with FDR-corrected $P < 0.05$ and related with metabolism were presented. **b**, Schema (top) and heatmap of relative intensity of significantly changed protein (bottom) in the oxidative phosphorylation pathway. **c**, Schema of metabolic pathways (pentose phosphate pathway, purine and pyrimidine metabolism) with select metabolites and proteins (top) and immunoblot analysis and protein quantification of HCM ($n = 16$) and non-HCM (ctrl) ($n = 8$) human cardiac tissue samples for G6PD (bottom). (All the samples derive from the same experiment and blots were processed in parallel.) Metabolites or proteins with significantly upregulated, downregulated and unchanged were colored in red, blue and black, respectively. Gray nodes represent metabolites or proteins that were not detected. Statistical analyses were performed by two-tailed unpaired Student's *t*-test and data were presented as mean ± sd. **d**, The schematic diagram illustrates the alterations of redox related proteins and metabolites in patients with HCM and the effects of *N*-acetylcysteine (NAC) to HCM animal models.

Discussion

HCM is highly heterogeneous and governed by multiple molecular mechanisms[5,8,10]. Disturbances in cardiac metabolism underlie most cardiovascular diseases[43,44]. However, the underlying metabolic alterations and their potential roles in HCM are largely unknown. Here, we presented a comprehensive metabolic characterization of human heart tissues and plasma from patients with HCM and non-HCM controls by using targeted metabolomics and lipidomics, which revealed the distinct metabolic profiles between patients with HCM and non-HCM controls. Beyond that, we identified a large number of metabolites that highly correlated with the heart function and prognosis of patients with HCM. Moreover, consensus clustering of metabolomics and lipidomics data identified three distinct metabolic subgroups of HCM. Finally, data resulting from integrative metabolomics and proteomic analyses suggested that interfering with the PPP and oxidative stress might represent potential therapeutic strategies for treatment of HCM.

Fatty acid oxidation (FAO) is the major resource for energy production in the heart[22,45] and previous studies have demonstrated that the hypertrophic and failing hearts reduce the utilization

of FAO while increase that of the glucose or other alternative substrates[18,28,46]. Fatty acids are produced by TAG hydrolysis or via de novo synthesis. Medium- and long-chain fatty acids conjugate with carnitine via carnitine palmitoyltransferase 1 (CPT1) and then translocate into mitochondria for β-oxidation[47]. Indeed, the CPT1 inhibitor-perhexiline significantly improves diastolic function, exercise capacity and cardiac energetics in patients with HCM[48]. Our data revealed that numerous carnitines were dramatically decreased in patients with HCM, indicating reduced mitochondrial fatty acid uptake. Moreover, our proteomics analysis identified that mitochondrial respiration chain complexes exhibited overall downregulation in patients with HCM. Thus, our data demonstrated that both substrates and 'machines' for the energy generation in FAO were dysregulated in patients with HCM.

Enhanced glucose utilization partially improves cardiac energetics, but does not mitigate cardiac hypertrophy[49,50]. In addition, recent studies showed that glucose is preferentially utilized for the biosynthesis of macromolecule rather than ATP generation during cardiac hypertrophy[29,51]. Our data suggested that glucose consumption not only supported glycolysis, but also entered into ancillary pathways such as PPP in patients with HCM. A previous study has demonstrated that the activity of the PPP rate-limiting enzyme-G6PD is dysregulated in desmin-related cardiomyopathy (DRM) mouse model and downregulation of G6PD abrogates the manifestations of DRM by reversing the redox imbalance[52]. Our data showed that both the protein level of G6PD and the intermediates of PPP, such as gluconate, were increased in patients with HCM. The upregulation of PPP may not be sufficient to reverse the imbalanced oxidative stress in patients with HCM, evidenced by the increase of GSSG; however, the upregulated PPP may consequentially promote the hypertrophy of cardiomyocytes by increasing purine and pyrimidine nucleotides.

Raised concentration of TAGs has been regarded as a causal risk factor for cardiovascular diseases[33]. A previous study indicated that TAGs with saturated fatty acids are more likely used for energy production[53]. In our study, we observed that most of TAGs were decreased in patients with HCM and TAGs with lower double-bond content were more significantly decreased, suggesting a deprivation of TAGs applicable for energy production in patients with HCM. In addition, we observed that patients with HCM showing a high proportion of TAGs with a low carbon number had poor survival outcomes, whereas patients showing a high proportion of TAGs with a high carbon number had better survival outcomes. Previous studies showed that TAGs with high carbon number were associated with a decreased risk of type 2 diabetes, whereas TAGs with low carbon number were associated with an increased risk of cardiovascular disease and type 2 diabetes[54,55], which indicated that the level/proportion of TAGs with different carbon number may serve as a good biomarker for the risk of different diseases.

Risk stratification effectively guides disease treatment decisions and surveillance[56]. Current risk stratification of patients with HCM, such as MWT[12,36], do not consider subtle pathophysiologic differences between patients with HCM. In contrast, metabolic clustering has been broadly applied to the risk stratification of cancers such as triple-negative breast cancer and clear cell renal cell carcinoma[57,58]. In this study, by using targeted metabolomics and lipidomics data, we performed a metabolic classification of patients with HCM and identified three metabolic subtypes of patients with HCM that feature distinct clinical characteristics including NYHA class and survival outcomes. Moreover, given that the relation between gene mutations and clinical outcomes has proved unreliable and there is no prognostic utility of a specific mutant gene[4,59] and according to our metabolomics and lipidomics data, myocardial metabolism was not clearly affected by genetic heterogeneity. We suggest that study of metabolites in an omics manner provides a perspective beyond gene mutations for understanding the complex heterogeneous phenotypes of HCM, which may facilitate the risk stratification and thereby shed light on precision treatment of the disease.

There are several limitations of our study. First, owing to the limited sample availability, only 16 non-HCM control samples were collected for metabolic study. Second, the patient cohort used in our study represents only a subclass of all patients with HCM and it is characterized by the indications of the myectomy for symptomatic left ventricular outflow tract gradient obstruction. Finally, given the high overall 5-year survival rate (95%)[60] of patients with HCM after surgery and our relatively short follow-up after surgery (4.5 ± 2.1 years), only 16 patients who died of HCM-related cardiovascular diseases were included in our study. Longer term follow-up may help understand the relationship between metabolism and prognosis more accurately and build a more effective machine learning model for the prediction of survival outcomes.

In summary, our study delineated the global metabolic alterations in the heart tissues and plasma of HCM; revealed two panels of metabolites that may serve as diagnostic for HCM and predictor for the survival outcomes of patients with HCM, respectively; identified three metabolic subtypes of patients with HCM; and highlighted potential therapeutic targets for HCM. Our work thus provides insights into the metabolic heterogeneity and pathogenesis of HCM that may potentially help understand the pathology, facilitate the development of rational therapeutic interventions and enable precision treatment for HCM.

Methods

Clinical sample acquisition. Left ventricular myocardium samples (septum) used for this study were collected from patients with obstructive HCM who underwent a Morrow septal myectomy at Fuwai Hospital, Chinese Academy of Medical Sciences and Peking Union Medical College. Human DCM left ventricular myocardium samples (septum) were obtained from patients with dilated cardiomyopathy undergoing cardiac transplantation at Tongji Hospital, Tongji Medical College, Wuhan, China. The HCM diagnosis was based on the following criteria: echocardiographic evidence of maximum left ventricular wall thickness of ≥15 mm, excluding patients with notable concomitant disease, HCM phenocopies and secondary hypertrophy (aortic stenosis, systemic hypertension)[61]. Left ventricular myocardium samples (septum) of 11 non-hypertrophic cardiomyopathy (non-HCM) were collected from healthy donor hearts that were obtained from explanted healthy hearts but not used for transplantation and 5 were collected from individuals who donated organs. All of the non-HCM controls had no history of cardiac diseases and therefore were used as control for HCM and DCM. The excised myocardium was immediately flash frozen in liquid nitrogen and stored in liquid nitrogen or −80 °C until used. Plasma samples of HCM were collected before surgery and plasma of non-HCM controls were collected from the physical examination population. Blood was drawn using BD Vacutainer EDTA tubes. The collected blood was centrifuged at 1,000*g* for 10 min at 4 °C and the supernatant as plasma. After aliquoting, plasma was frozen at −80 °C until metabolite extraction. This study was approved by the Ethics Committee of Fuwai Hospital, Chinese Academy of Medical Science and Peking Union Medical College, Beijing, China and Tongji Hospital, Tongji Medical College. Written informed consent was obtained from all the participants or their relatives and they also agreed that the data and information obtained from patients' tissues and plasma could be used in a publication. The baseline clinical characteristics of patients with HCM were collected at enrollment. Left ventricle wall thickness, left ventricular outflow tract gradient and left ventricular ejection fraction were all assessed by echocardiography, which was performed before myectomy therapy. Meanwhile, all patients were followed-up annually until July 2020 by a clinic visit or telephone interview. The follow-up time extended from the first evaluation until death from any cause or the last known contact date. The end point of the study was cardiovascular death, including sudden cardiac death and death induced by heart failure and stroke. Resuscitation from cardiac arrest and appropriate implantable cardioverter-defibrillator shock therapy for ventricular tachycardia or fibrillation were considered to be equivalent to sudden cardiac death.

Genotyping. The sarcomere pathogenic genes of HCM, including *MYH7*, *MYBPC3*, *TNNT2*, *TNNI3*, *MYL2*, *MYL3*, *TPM1* and *ACTC1* were genotyped by WES or panel sequencing as previously reported[62,63]. Briefly, WES was performed on Illumina NovaSeq platform as the manufacturer's protocols using the Agilent Sure SelectXT Human All Exon V6 kit[62]. For panel sequencing, genomic DNA library were constructed and targeted-exonic regions were enriched using a custom-designed probe library, followed by sequencing on Illumina GAIIx[63]. The obtained reads were aligned to the human reference genome and variants were called using Genome Analysis Toolkit (v.3.7). The SnpEff software (v.4.3) was used

to annotate variants to canonical transcripts. The pathogenicity of variants detected in eight sarcomere pathogenic genes were classified according to the criteria of American College of Medical Genetics and Genomics[64].

Metabolite extraction. Samples extraction for targeted metabolomics analysis: each tissue sample was accurately weighed and homogenized in ice-cold 80% methanol aqueous solution (50 mg tissue per ml). The 100 µl of tissue homogenate was mixed with ice-cold 900 µl 80% methanol aqueous solution. The mixture was then vortexed and centrifuged at 20,000*g* for 15 min at 4 °C and 900 µl supernatant was transferred to a new tube. The pellet was mixed with 500 µl ice-cold 80% methanol and re-centrifuged at 20,000*g* for 15 min at 4 °C; 500 µl supernatant was collected and combined with the previous supernatant. The mixed supernatant was vortexed and divided into two new tubes with equal volume. The supernatant was dried with SpeedVac (Thermo Scientific) and the dried metabolite extracts were stored at −80 °C until LC–MS analysis. QC samples were prepared by pooling 20 µl homogenate of each tissue sample. Pretreatment of QC samples was paralleled and same to the study samples.

For metabolite extraction of plasma samples, 60 µl plasma of each person was mixed with 240 µl ice-cold methanol. The mixture was then vortexed and centrifuged at 20,000*g* for 15 min at 4 °C. The supernatant was divided into two replicates and evaporated to dryness with SpeedVac. For QC sample preparation, 20 µl plasma of each person was mixed and then processed the same as that of the study plasma samples.

Samples extraction for lipidomics analysis was performed as previously described with some modification[65]. Briefly, for polar lipid extraction (such as FFA, PC and PE), 10 µl tissue homogenate was mixed with 50 µl ice-cold isopropanol (IPA). Samples were vortexed briefly and then incubated for 2 h at 4 °C. After incubation, samples were centrifuged at 20,000*g* for 10 min at 4 °C, 50 µl supernatant was transferred to glass vials for liquid chromatography–mass spectrometry (LC–MS) analysis. For TAG extraction, 10 µl tissue homogenate was mixed with 40 µl ice-cold methanol. After vortexing briefly and incubating for 10 min at 4 °C, samples were centrifuged at 20,000*g* for 10 min at 4 °C; 40 µl supernatant was diluted with 40 µl of deionized water and mixed for LC–MS analysis. QC samples were prepared by pooling 20 µl homogenate of each tissue sample. Pretreatment of QC samples was paralleled and the same as the study samples.

Targeted metabolomics analysis. The dried metabolites were reconstituted in 50 µl of 0.03% formic acid in water, vortexed, centrifuged at 20,000*g* for 15 min at 4 °C and the supernatant was analyzed using LC–MS/MS. An ultra-high-performance liquid chromatography system (Nexera×2 LC-30A, Shimadzu) was used for liquid chromatography, with an ACQUITY UPLC HSS-T3 UPLC column (150 × 2.1 mm, 1.8 µm, Waters) and the following gradient: 0–3 min 1% mobile phase B; 3–15 min 1–99% B; 15–17 min 99% B; 17–17.1 min 99–1% B; and 17.1–20 min 1% B. Mobile phase A was 0.03% formic acid in water and mobile phase B was 0.03% formic acid in acetonitrile (ACN). The flow rate was 0.25 ml min^{-1}, the column was at 35 °C and the samples in the auto sampler were at 4 °C. The injection volume was 10 µl. MS was performed with a triple quadrupole mass spectrometer (Qtrap 6500$^+$, Sciex) in multiple reaction-monitoring (MRM) mode. Sample analysis was performed under a positive/negative switching mode, a total of 251 metabolites were monitored with 158 ion transitions in positive mode and 93 ion transitions in negative mode as previously described[66], with some modifications. Samples were analyzed in a randomized order, with QC samples evenly inserted in each batch of the acquisition sequence per 10–20 samples to monitor the stability of the large-scale metabolomics analysis. Chromatogram review and peak area integration were performed using MultiQuant software v.3.0 (Sciex).

Lipidomics analysis. Lipidomics were analyzed using the LipidQuan platform (Waters) that comprises a Xevo TQ-XS mass spectrometer (Waters) and an ACQUITY UPLC I-Class system (Waters). For polar lipids analysis, UPLC separation was performed on an ACQUITY BEH Amide column (100 × 2.1 mm, 1.7 µm, Waters) at 45 °C. The mobile phases were 95% ACN in water with 10 mM ammonium acetate (mobile phase A) and 50% ACN in water with 10 mM ammonium acetate (mobile phase B). The gradient was 0–2 min 0.1–20.0% B, 2–5 min 20.0–80.0% B, 5–5.1 min 80.0–0.1% B and 5.1–8 min 0.1% B. The flow rate was set at 0.6 ml min^{-1} and the injection volume was 1 µl. MS was performed using a MRM mode with positive (CE, SM, LPC, LPE, Cer, HexCer, PC, DAG) or negative (FFA, PE, PG, PS, PI, PC) electrospray ionization mode. The ion source temperature and desolvation temperature were set as 150 °C and 650 °C, respectively and the capillary voltage was kept at 2.8 kV for positive mode and 1.9 kV for negative mode. For TAG analysis, samples were separated with a CORTECS T3 column (30 × 2.1 mm, 2.7 µm, Waters). The 2-µl sample was injected and the flow rate was 0.25 ml min^{-1}. Mobile phase A was 0.01% formic acid containing 0.2 mM ammonium formate and mobile phase B was 50% IPA in ACN containing 0.01% formic acid and 0.2 mM ammonium formate. The gradient was set as 0–2 min 90% B, 2–6 min 90–98% B, 6–8 min 98% B, 8–8.1 min 98–90% B and 8.1–10 min 90% B. All TAGs were performed in positive mode with MRM mode. The ion source temperature and capillary voltage were kept constant at 150 °C and 2.0 kV, respectively and the desolvation temperature was 650 °C. All samples were acquired in a random order with QC samples evenly inserted in each batch of the acquisition sequence per 12–20 samples to monitor the stability of the large-scale lipidomics analysis. Chromatogram review and peak area integration were performed using Skyline software (MacCoss Lab).

Targeted metabolomics and lipidomics data processing. Data processing was performed as previously described[67]. Briefly, the mean peak area of each metabolite from all QC samples in all given batches (QCall), as well as the mean peak area of each metabolite from the QC samples that were the most adjacent to a given group of test samples (QCadj) were first calculated. The ratio between these two mean peak areas for each metabolite was computed by dividing the same QCall by each QCadj and used as the normalization factor for each given group of test samples. The peak area of each metabolite from each test sample was normalized by multiplying their corresponding normalization ratio to obtain the normalized peak areas to remove potential batch variations. In addition, to effectively correct the sample-to-sample variation in biomass that may contribute to systematic differences in metabolites abundance detected by LC–MS, we generated the scaled data by comparing the normalized peak area of each metabolite to the sum of the normalized peak area from all the detected metabolites in that given sample (excluding TAGs).

Detection of metabolites in glycolysis pathway by 3-NPZ derivatization. Measurement of key metabolites in glycolysis was performed as previously described[68,69]. Briefly, the dried metabolite extracts were derivatization with 3-nitrophenylhydrazine (3-NPZ) and injected for chromatographic separation on an ACQUITY UPLC HSS-T3 UPLC column (150 × 2.1 mm, 1.8 µm, Waters) followed by detection and measurement using a Qtrap 6500$^+$ mass spectrometer equipped with an electrospray ionization source.

Proteomics analysis. Seven male non-HCM control samples were separated into four control groups, including one group with one sample and three groups with two pooled samples per group. Sixty-three male HCM samples were used to pool into six HCM groups with 10–12 samples per group. Tissue samples were ground to a powder in liquid nitrogen and then lysed in 8 M urea containing 1% protease inhibitor cocktail and then sonicated using a high-intensity ultrasonic processor (Scientz) three times and centrifuged at 12,000*g* at 4 °C for 10 min. The supernatant was collected and protein content was quantified using a BCA Protein Assay kit (Beyotime). The proteins were then reduced and alkylated by mixing sequentially with 5 mM dithiothreitol at 56 °C for 30 min and with 11 mM iodoacetamide at room temperature for 15 min in the dark. The protein sample was diluted by addition of 100 mM tetraethylammonium bromide (TEAB) to give a final urea concentration of <2 M. Trypsin was added at a 1:50 trypsin-to-protein mass ratio overnight followed by a second digestion for 4 h at a 1:100 ratio. Peptides were desalted using a Strata X C18 SPE column from Phenomenex and then vacuum-dried. The peptides were reconstituted in 0.5 M TEAB and processed using a TMT 10 plex kit (Thermo Fisher, 90406LCS). The peptides were then fractionated using high pH RP-HPLC on an Agilent 300Extend C18 column (5-µm particle size, 4.6-mm internal diameter (i.d.) and 250 mm length), combined into 18 fractions and dried by vacuum centrifugation. Peptides from each fraction were dissolved in 0.1% formic acid (solvent A) and loaded onto a homemade RP-HPLC analytical column (75-µm i.d. and 150 mm length). The peptides were separated using an EASY-nLC 1000 UPLC system with the following gradient: 6% to 23% solvent B (0.1% formic acid in 98% acetonitrile) over 26 min, 23% to 35% over 8 min and 35% to 80% over 3 min, followed by a hold at 80% for 3 min. The flow rate was constant at 400 nl min^{-1}. The peptides were analyzed using an Q ExactiveTM Plus MS/MS system (Thermo Scientific, Pierce Protein Biology Products) coupled online to the UPLC. The peptides were selected for MS/MS using a normalized collision energy setting of 28 and the fragments were detected in the Orbitrap at a resolution of 17,500 with a fixed first mass set at 100 m/z. The TMT reporter ions were measured in high-resolution MS2 mode and the interference was controlled by FDR and score cutoff. The cutoffs for modified peptides, score for recalibration and the FDR of peptide level were 40, 70 and 0.01, respectively. The raw MS/MS data were analyzed using the Maxquant search engine (v.1.5.2.8). Tandem mass spectra were searched against the SwissProt Human database (20,317 sequences) concatenated with a reverse decoy database. Trypsin/P was specified as the cleavage enzyme, allowing up to two missing cleavages. In the first and main searches, the mass tolerance of precursor ions was set at 5 ppm and 20 ppm, respectively and the mass tolerance for fragment ions was set at 0.02 Da.

Identification of differential metabolites and proteins in patients with HCM. Statistical differences of the metabolites were analyzed by R stat (v.3.6.3) package using Mann–Whitney *U*-test (two-sided) and followed by Benjamini–Hochberg (BH) multiple comparisons test (FDR). Statistical differences of proteins were analyzed by Excel (v.2016) using Student's *t*-test (two-sided) and followed by Benjamini–Hochberg multiple comparisons test. Metabolites with FDR-corrected $P < 0.05$, FC >1.5 or <0.67, were considered as differential and used for subsequent analysis. Proteins with FDR-corrected $P < 0.05$ were considered as differential and used for subsequent analysis.

KEGG pathway analysis. KEGG metabolic pathways and involved metabolites were downloaded from KEGG API (https://www.kegg.jp/kegg/rest/keggapi.html). Significant enriched KEGG pathways were determined by R clusterProfiler

(v.3.12.0) package[70] with Fisher's exact test followed by BH multiple comparison test as FDR-corrected $P < 0.05$ and enriched for at least two metabolites (for differential metabolites). Significant enriched KEGG pathways for proteins were performed in Database for Annotation, Visualization and Integrated Discovery (v.6.8) (https://david.ncifcrf.gov) with Fisher's exact test followed by BH multiple comparison test as FDR-corrected $P < 0.05$ and enriched for at least five proteins (for differential proteins).

PCA and PLS-DA for metabolomics and lipidomics data. PCA and PLS-DA were performed by the prcomp and plsda function under R stat (v.3.6.3) and mixOmics (v.6.8.5) package using the $\log_2$ transformed abundance matrixes of global metabolites, respectively. To evaluate the robustness of the results, we evaluated the PLS-DA model by the perf function under R mixOmics packages[71]. The 95% confidence interval was represented by ellipses, which was calculated based on the mean and covariance of points in each group.

Correlation analysis of differential metabolites. Correlation between differential metabolites abundance for each metabolite-metabolite pair across all 349 patients with HCM were calculated by Spearman correlation method using the cor function under R stat (v.3.6.3) package. In addition, *P* value corresponding to the correlation coefficient was computed by the cor_pmat function under R stat (v.3.6.3) package. Differential metabolites with a correlation coefficient >0.5 or <−0.5 were imported into Cytoscape (v.3.8.0) software to create coexpression networks[72].

Logistic regression analysis. Logistic regression model with covariates body mass index, age and sex were built with each metabolite to search for significant metabolites that associated with the NYHA class. The ORs were estimated by the glm function under R stat (v.3.6.3) package. *P* value of the variable estimate in the model were computed by the Wald test and adjusted by the FDR correction.

Association between metabolites and clinical outcome. Survival analysis was performed using R survival (v.3.1-11) package. The median of metabolite abundances as the cutoff for expression dichotomization. For the association of metabolites level with survival, a log-rank test was used to compare overall survival outcomes between two groups and among three clusters generated by metabolomics and lipidomics. For all analyses, significant association with survival was achieved for $P < 0.05$. Kaplan–Meier survival curves were plotted by function ggsurvplot in R survminer (v.0.4.6) package.

Machine learning for the diagnosis of HCM and prediction of survival outcomes. For the diagnosis of HCM, we first performed least absolute shrinkage and selection operator (LASSO) to select a reduced number of features which were diagnosis enough for the HCM on the training dataset and then we conducted fivefold cross validation on the training set ten times with different random seeds to obtain stable feature selection results. We set the coefficient of L1 constraint to 0.001 and selected the features which had a nonzero coefficient[73]. For the prediction of survival outcomes, 302 patients (286 participants survived after surgery and 16 participants deceased after surgery) were divided into the training set and testing set according to the chronological order of sample collection. The features were selected based on their variable importance. Once the feature selection was finished, we built a diagnosis/prediction model by using random forests (RF)/random survival forests (RSF) method based on the training dataset. Then diagnosis and prediction model was applied to diagnose HCM and predict the survival outcomes in the testing set[74,75]. One hundred trees were built using the criterion of Gini impurity for RF analysis and 1,000 trees were built using log-rank test for RSF analysis. LASSO and RF were performed via the scikit-learn package (v.0.24.1) and RSF was performed via the scikit-survival package (v.0.17.1) in Python (v.3.7.4).

Metabolomics and lipidomics consensus clustering. *K*-means consensus clustering was performed on metabolomics and lipidomics data with no missing values to generate subgroups using R ConsensusClusterPlus (v.1.48.0) package[76] and the following detail settings were used for clustering: number of repetitions, 1,000 bootstraps; pItem, 0.8; and pFeature, 0.8. *K*-means clustering range from $k = 2$–6. The optimizing *K*-means clustering was ascertained by the average pairwise consensus matrix within consensus clusters and the delta plot of the relative change in the area under the cumulative distribution function curve. Based on the evidence mentioned above, the metabolomics and lipidomics data of patients with HCM were clustered into three subtypes.

Cluster related metabolic changes. Kruskal–Wallis tests with Dunn's multiple comparison test by R dunn.test (v.1.3.5) package was used to obtain the significantly altered metabolites in each cluster, relative to other two clusters. Metabolites with FDR-corrected $P < 0.05$, FC >1.25 or <0.8, were considered as differential metabolites and used for subsequent analysis. The average absolute $\log_2$ FC of differential metabolites enriched in each KEGG pathway was calculated.

Immunoblot analysis. Human cardiac tissues of 10–15 mg were homogenized in 500 µl RIPA (Solarbio) supplemented with protease and phosphate inhibitor (Biomake). Tissue lysate samples were centrifuged at 15,000*g* for 10 min at 4 °C and protein concentration was measured using a BCA protein assay kit (Beyotime). Samples were heated at 95 °C for 20 min in loading buffer. Equal amounts of total proteins were subject to SDS–PAGE gels and transferred to PVDF membranes (GE Amersham). Membranes were blocked with 5% nonfat milk (Bioruler) in PBS-Tween for 1 h at room temperature and then probed with the appropriate antibodies at 4 °C overnight. Primary antibodies used for western blot analysis were anti-GAPDH (Proteintech, 60004-1-lg, 1:5,000 dilution) and anti-G6PD (Sigma, HPA000834, 1:1,000 dilution). After that, the appropriate secondary antibody (CST, anti-mouse, 7076S; anti-rabbit, 7074S; 1:5,000 dilution) conjugated with horseradish peroxidase was added to incubate for 1 h at room temperature. A chemiluminescence blotting system (Pierce) was used for detection. The western blot gel image was obtained with a chemiluminescent imager (Tanon5200).

Statistical analysis. All statistical methods used were listed in the figure legends or corresponding methods. Mann–Whitney *U*-test and Student's *t*-test were used to compare two groups of independent samples. To account for multiple testing, the *P* values were adjusted using the FDR correction. For categorical variables versus categorical variables, Fisher's exact test was used. Kruskal–Wallis tests with Dunn's multiple comparison test was used to test whether any of the differences between the subgroups were statistically significant. No statistical methods were used to predetermine sample sizes but our sample sizes are similar to those reported in previous publications[77,78]. All the analyses of clinical data were performed in R (v.3.6.3), Excel (v.2016) and GraphPad Prism (v.8.0).

Reporting Summary. Further information on research design is available in the Nature Research Reporting Summary linked to this article.

Data availability

The clinical information of each HCM patient is provided in Supplementary Table 1. The baseline clinical characteristics for DCM and non-HCM controls are included in Supplementary Table 2. As public sharing of the raw genomic data is restricted by the regulation of the Human Genetic Resources Administration of China, detailed results of WES are included in Supplementary Table 3. Raw metabolomics and lipidomics data are included in Supplementary Tables 4–6. The MS proteomics raw data is deposited in the ProteomeXchange Consortium (http://proteomecentral.proteomexchange.org) via the iProX partner repository with dataset identifier PXD032097. Source data are provided with this paper.

Code availability

Codes for data analysis are available at https://github.com/WenminWang15/HCM_Nat-Cardiovasc-Res.

Received: 19 July 2021; Accepted: 28 March 2022;
Published online: 9 May 2022

References

1. Maron, B. J. Clinical course and management of hypertrophic cardiomyopathy. *New Engl. J. Med.* **379**, 655–668 (2018).
2. Semsarian, C., Ingles, J., Maron, M. S. & Maron, B. J. New perspectives on the prevalence of hypertrophic cardiomyopathy. *J. Am. Coll. Cardiol.* **65**, 1249–1254 (2015).
3. Virani, S. S. et al. Heart disease and stroke statistics 2021 update: a report from the American heart association. *Circulation* **143**, e254–e743 (2021).
4. Maron, B. J. & Maron, M. S. Hypertrophic cardiomyopathy. *Lancet* **381**, 242–255 (2013).
5. Sen-Chowdhry, S., Jacoby, D., Moon, J. C. & McKenna, W. J. Update on hypertrophic cardiomyopathy and a guide to the guidelines. *Nat. Rev. Cardiol.* **13**, 651–675 (2016).
6. Marian, A. J. & Braunwald, E. Hypertrophic cardiomyopathy: genetics, pathogenesis, clinical manifestations, diagnosis, and therapy. *Circ. Res.* **121**, 749–770 (2017).
7. Alfares, A. A. et al. Results of clinical genetic testing of 2,912 probands with hypertrophic cardiomyopathy: expanded panels offer limited additional sensitivity. *Genet. Med.* **17**, 880–888 (2015).
8. Frey, N., Luedde, M. & Katus, H. A. Mechanisms of disease: hypertrophic cardiomyopathy. *Nat. Rev. Cardiol.* **9**, 91–100 (2011).
9. Ormerod, J. O., Frenneaux, M. P. & Sherrid, M. V. Myocardial energy depletion and dynamic systolic dysfunction in hypertrophic cardiomyopathy. *Nat. Rev. Cardiol.* **13**, 677–687 (2016).
10. Maron, B. J., Maron, M. S., Maron, B. A. & Loscalzo, J. Moving beyond the sarcomere to explain heterogeneity in hypertrophic cardiomyopathy: JACC review topic of the week. *J. Am. Coll. Cardiol.* **73**, 1978–1986 (2019).
11. Maurizi, N. et al. Clinical course and significance of hypertrophic cardiomyopathy without left ventricular hypertrophy. *Circulation* **139**, 830–833 (2019).
12. Elliott, P. M. et al. 2014 ESC guidelines on diagnosis and management of hypertrophic cardiomyopathy: the Task Force for the Diagnosis and

Management of Hypertrophic Cardiomyopathy of the European Society of Cardiology (ESC). *Eur. Heart J.* **35**, 2733–2779 (2014).
13. Kurilshikov, A. et al. Gut microbial associations to plasma metabolites linked to cardiovascular phenotypes and risk. *Circ. Res.* **124**, 1808–1820 (2019).
14. Nicholson, G. et al. Human metabolic profiles are stably controlled by genetic and environmental variation. *Mol. Syst. Biol.* **7**, 525 (2011).
15. Pang, H., Jia, W. & Hu, Z. Emerging applications of metabolomics in clinical pharmacology. *Clin. Pharmacol. Ther.* **106**, 544–556 (2019).
16. Liang, L., Sun, F., Wang, H. & Hu, Z. Metabolomics, metabolic flux analysis and cancer pharmacology. *Pharmacol. Ther.* **224**, 107827 (2021).
17. Wishart, D. S. Emerging applications of metabolomics in drug discovery and precision medicine. *Nat. Rev. Drug Discov.* **15**, 473–484 (2016).
18. Bertero, E. & Maack, C. Metabolic remodelling in heart failure. *Nat. Rev. Cardiol.* **15**, 457–470 (2018).
19. Ussher, J. R., Elmariah, S., Gerszten, R. E. & Dyck, J. R. The emerging role of metabolomics in the diagnosis and prognosis of cardiovascular disease. *J. Am. Coll. Cardiol.* **68**, 2850–2870 (2016).
20. Zhu, J. & Thompson, C. B. Metabolic regulation of cell growth and proliferation. *Nat. Rev. Mol. Cell Biol.* **20**, 436–450 (2019).
21. Davis, J. et al. A tension-based model distinguishes hypertrophic versus dilated cardiomyopathy. *Cell* **165**, 1147–1159 (2016).
22. Lopaschuk, G. D., Ussher, J. R., Folmes, C. D., Jaswal, J. S. & Stanley, W. C. Myocardial fatty acid metabolism in health and disease. *Physiol. Rev.* **90**, 207–258 (2010).
23. Madeo, F., Eisenberg, T., Pietrocola, F. & Kroemer, G. Spermidine in health and disease. *Science* **359**, eaan2788 (2018).
24. Percudani, R. & Peracchi, A. A genomic overview of pyridoxal-phosphate-dependent enzymes. *EMBO Rep.* **4**, 850–854 (2003).
25. Marian, A. J., Senthil, V., Chen, S. N. & Lombardi, R. Antifibrotic effects of antioxidant N-acetylcysteine in a mouse model of human hypertrophic cardiomyopathy mutation. *J. Am. Coll. Cardiol.* **47**, 827–834 (2006).
26. Lombardi, R. et al. Resolution of established cardiac hypertrophy and fibrosis and prevention of systolic dysfunction in a transgenic rabbit model of human cardiomyopathy through thiol-sensitive mechanisms. *Circulation* **119**, 1398–1407 (2009).
27. Gibb, A. A. & Hill, B. G. Metabolic coordination of physiological and pathological cardiac remodeling. *Circ. Res.* **123**, 107–128 (2018).
28. Ritterhoff, J. & Tian, R. Metabolism in cardiomyopathy: every substrate matters. *Cardiovasc. Res.* **113**, 411–421 (2017).
29. Ritterhoff, J. et al. Metabolic remodeling promotes cardiac hypertrophy by directing glucose to aspartate biosynthesis. *Circ. Res.* **126**, 182–196 (2020).
30. Dyar, K. A. et al. Atlas of circadian metabolism reveals system-wide coordination and communication between clocks. *Cell* **174**, 1571–1585 (2018).
31. Gottlieb, E. & Tomlinson, I. P. Mitochondrial tumour suppressors: a genetic and biochemical update. *Nat. Rev. Cancer* **5**, 857–866 (2005).
32. Hilvo, M. et al. Development and validation of a ceramide- and phospholipid-based cardiovascular risk estimation score for coronary artery disease patients. *Eur. Heart J.* **41**, 371–380 (2020).
33. Nordestgaard, B. G. & Varbo, A. Triglycerides and cardiovascular disease. *Lancet* **384**, 626–635 (2014).
34. Russo, S. B. et al. Ceramide synthase 5 mediates lipid-induced autophagy and hypertrophy in cardiomyocytes. *J. Clin. Invest.* **122**, 3919–3930 (2012).
35. Haq, S. et al. Deletion of cytosolic phospholipase A2 promotes striated muscle growth. *Nat. Med.* **9**, 944–951 (2003).
36. Ommen, S. R. et al. 2020 AHA/ACC guideline for the diagnosis and treatment of patients with hypertrophic cardiomyopathy: executive summary: a report of the American College of Cardiology/American Heart Association Joint Committee on Clinical Practice Guidelines. *Circulation* **142**, e533–e557 (2020).
37. Heggermont, W. A. et al. Inhibition of MicroRNA-146a and overexpression of its target dihydrolipoyl succinyltransferase protect against pressure overload-induced cardiac hypertrophy and dysfunction. *Circulation* **136**, 747–761 (2017).
38. Li, Q. et al. PKM1 exerts critical roles in cardiac remodeling under pressure overload in the heart. *Circulation* **144**, 712–727 (2021).
39. Stanley, W. C., Recchia, F. A. & Lopaschuk, G. D. Myocardial substrate metabolism in the normal and failing heart. *Physiol. Rev.* **85**, 1093–1129 (2005).
40. Huang, J. M., Xian, H. & Bacaner, M. Long-chain fatty acids activate calcium channels in ventricular myocytes. *PNAS* **89**, 6452–6456 (1992).
41. Stincone, A. et al. The return of metabolism: biochemistry and physiology of the pentose phosphate pathway. *Biol. Rev. Camb. Philos. Soc.* **90**, 927–963 (2015).
42. Dimitrow, P. P., Undas, A., Wołkow, P., Tracz, W. & Dubiel, J. S. Enhanced oxidative stress in hypertrophic cardiomyopathy. *Pharmacol. Rep.* **61**, 491–495 (2009).
43. McGarrah, R. W., Crown, S. B., Zhang, G. F., Shah, S. H. & Newgard, C. B. Cardiovascular metabolomics. *Circ. Res.* **122**, 1238–1258 (2018).
44. Taegtmeyer, H. et al. Assessing cardiac metabolism: a scientific statement from the American Heart Association. *Circ. Res.* **118**, 1659–1701 (2016).
45. Murashige, D. et al. Comprehensive quantification of fuel use by the failing and nonfailing human heart. *Science* **370**, 364–368 (2020).
46. Lionetti, V., Stanley, W. C. & Recchia, F. A. Modulating fatty acid oxidation in heart failure. *Cardiovasc. Res.* **90**, 202–209 (2011).
47. Carracedo, A., Cantley, L. C. & Pandolfi, P. P. Cancer metabolism: fatty acid oxidation in the limelight. *Nat. Rev. Cancer* **13**, 227–232 (2013).
48. Abozguia, K. et al. Metabolic modulator perhexiline corrects energy deficiency and improves exercise capacity in symptomatic hypertrophic cardiomyopathy. *Circulation* **122**, 1562–1569 (2010).
49. Liao, R. et al. Cardiac-specific overexpression of GLUT1 prevents the development of heart failure attributable to pressure overload in mice. *Circulation* **106**, 2125–2131 (2002).
50. Shao, D. et al. Glucose promotes cell growth by suppressing branched-chain amino acid degradation. *Nat. Commun.* **9**, 2935 (2018).
51. Umbarawan, Y. et al. Glucose is preferentially utilized for biomass synthesis in pressure-overloaded hearts: evidence from fatty acid-binding protein-4 and -5 knockout mice. *Cardiovasc. Res.* **114**, 1132–1144 (2018).
52. Rajasekaran, N. S. et al. Human αB-crystallin mutation causes oxido-reductive stress and protein aggregation cardiomyopathy in mice. *Cell* **130**, 427–439 (2007).
53. Contrepois, K. et al. Molecular choreography of acute exercise. *Cell* **181**, 1112–1130 (2020).
54. Rhee, E. P. et al. Lipid profiling identifies a triacylglycerol signature of insulin resistance and improves diabetes prediction in humans. *J. Clin. Invest.* **121**, 1402–1411 (2011).
55. Stegemann, C. et al. Lipidomics profiling and risk of cardiovascular disease in the prospective population-based Bruneck study. *Circulation* **129**, 1821–1831 (2014).
56. Schwartz, P. J. et al. Inherited cardiac arrhythmias. *Nat. Rev. Dis. Primers.* **6**, 58 (2020).
57. Gong, Y. et al. Metabolic-pathway-based subtyping of triple-negative breast cancer reveals potential therapeutic targets. *Cell Metab.* **33**, 51–64 (2021).
58. Hakimi, A. A. et al. An integrated metabolic atlas of clear cell renal cell carcinoma. *Cancer Cell* **29**, 104–116 (2016).
59. Landstrom, A. P. & Ackerman, M. J. Mutation type is not clinically useful in predicting prognosis in hypertrophic cardiomyopathy. *Circulation.* **122**, 2441–2449 (2010).
60. Ball, W. et al. Long-term survival in patients with resting obstructive hypertrophic cardiomyopathy comparison of conservative versus invasive treatment. *J. Am. Coll. Cardiol.* **58**, 2313–2321 (2011).
61. Gersh, B. J. et al. 2011 ACCF/AHA guideline for the diagnosis and treatment of hypertrophic cardiomyopathy: executive summary: a report of the American College of Cardiology Foundation/American Heart Association task force on practice guidelines. *Circulation* **124**, 2761–2796 (2011).
62. Wu, G. et al. Variant spectrum of formin homology 2 domain-containing 3 gene in chinese patients with hypertrophic cardiomyopathy. *J. Am. Heart Assoc.* **10**, e018236 (2021).
63. Wang, J. et al. Malignant effects of multiple rare variants in sarcomere genes on the prognosis of patients with hypertrophic cardiomyopathy. *Eur. J. Heart Fail.* **16**, 950–957 (2014).
64. Richards, S. et al. Standards and guidelines for the interpretation of sequence variants: a joint consensus recommendation of the American College of Medical Genetics and Genomics and the Association for Molecular Pathology. *Genet. Med.* **17**, 405–424 (2015).
65. Sarafian, M. H. et al. Objective set of criteria for optimization of sample preparation procedures for ultra-high throughput untargeted blood plasma lipid profiling by ultra performance liquid chromatography–mass spectrometry. *Anal. Chem.* **86**, 5766–5774 (2014).
66. Huang, F. et al. Inosine monophosphate dehydrogenase dependence in a subset of small cell lung cancers. *Cell Metab.* **28**, 369–382 (2018).
67. Xiao, N. et al. Integrated cytokine and metabolite analysis reveals immunometabolic reprogramming in COVID-19 patients with therapeutic implications. *Nat. Commun.* **12**, 1618 (2021).
68. Han, J., Gagnon, S., Eckle, T. & Borchers, C. H. Metabolomic analysis of key central carbon metabolism carboxylic acids as their 3-nitrophenylhydrazones by UPLC/ESI-MS. *Electrophoresis* **34**, 2891–2900 (2013).
69. Meng, X. et al. Simultaneous 3-nitrophenylhydrazine derivatization strategy of carbonyl, carboxyl and phosphoryl submetabolome for LC–MS/MS-based targeted metabolomics with improved sensitivity and coverage. *Anal. Chem.* **93**, 10075–10083 (2021).
70. Yu, G., Wang, L. G., Han, Y. & He, Q. Y. clusterProfiler: an R package for comparing biological themes among gene clusters. *Omics* **16**, 284–287 (2012).
71. Rohart, F., Gautier, B., Singh, A. & KA, L. C. mixOmics: an R package for 'omics feature selection and multiple data integration. *PLoS Comput. Biol.* **13**, e1005752 (2017).
72. Shannon, P. et al. Cytoscape: a software environment for integrated models of biomolecular interaction networks. *Genome Res.* **13**, 2498–2504 (2003).

73. Tibshirani, R. Regression shrinkage and selection via the lasso. *J. R. Stat. Soc. B Methodol.* **58**, 267–288 (1996).
74. Breiman, L. Random forests. *Mach. Learn.* **45**, 5–32 (2001).
75. Ishwaran, H., Kogalur, U. B., Blackstone, E. H. & Lauer, M. S. Random survival forests. *Ann. Appl. Stat.* **2**, 841-860 (2008).
76. Wilkerson, M. D. & Hayes, D. N. ConsensusClusterPlus: a class discovery tool with confidence assessments and item tracking. *Bioinformatics* **26**, 1572–1573 (2010).
77. van Heesch, S. et al. The translational landscape of the human heart. *Cell* **178**, 242–260 (2019).
78. Nie, M. et al. Evolutionary metabolic landscape from preneoplasia to invasive lung adenocarcinoma. *Nat. Commun.* **12**, 6479 (2021).

Acknowledgements

We thank the members of the Hu laboratory for critiquing the manuscript and N. Xiao, J. Li, B. Peng, S. Mao and T. Xu for their helpful discussion. This study is supported by grants from the National Natural Science Foundation of China (32150024, 92057209) (received by Z.H.), (81870286) (received by L.S.), the CAMS Fund for Young Talents of Medical Science (2018RC310006) (received by J.W.), the CAMS Innovation Fund for Medical Sciences (CAMS-2020-I2M-C&T-A-006) (received by L.S.), National Key R&D Program of China (2020YFA0803300) (received by Z.H.), and Tsinghua-Peking Center for Life Sciences, Beijing Frontier Research Center for Biological Structure (received by Z.H.).

Author contributions

W.W. and Z.H. designed the study and wrote the manuscript. W.W. performed data analyses, data integration and western blot experiments. K.Y. and W.W. performed targeted metabolomics experiments and data processing. K.Y. and J.X. performed lipidomics experiments and data processing. J.W., G.W. and M.L. performed WES and proteomics experiments. M.N., Y.Z., B.W., H.P. and P.L. assisted in data interpretation and manuscript editing. N.T., C.Q., Y.L., Q.S., X.W., D.J., J.W., G.W., S.W. and L.S. provided clinical samples and information. Y.Z., H.P., X,L., D.L. and T.Y. performed machine learning. Z.H. conceived and supervised the project.

Competing interests

The authors declare no competing interests.

Additional information

Extended data is available for this paper at https://doi.org/10.1038/s44161-022-00057-1.

Supplementary information The online version contains supplementary material available at https://doi.org/10.1038/s44161-022-00057-1.

Correspondence and requests for materials should be addressed to Jizheng Wang, Lei Song or Zeping Hu.

Peer review information *Nature Cardiovascular Research* thanks Nicholas Larson and the other, anonymous, reviewers for their contribution to the peer review of this work.

Reprints and permissions information is available at www.nature.com/reprints.

Publisher's note Springer Nature remains neutral with regard to jurisdictional claims in published maps and institutional affiliations.

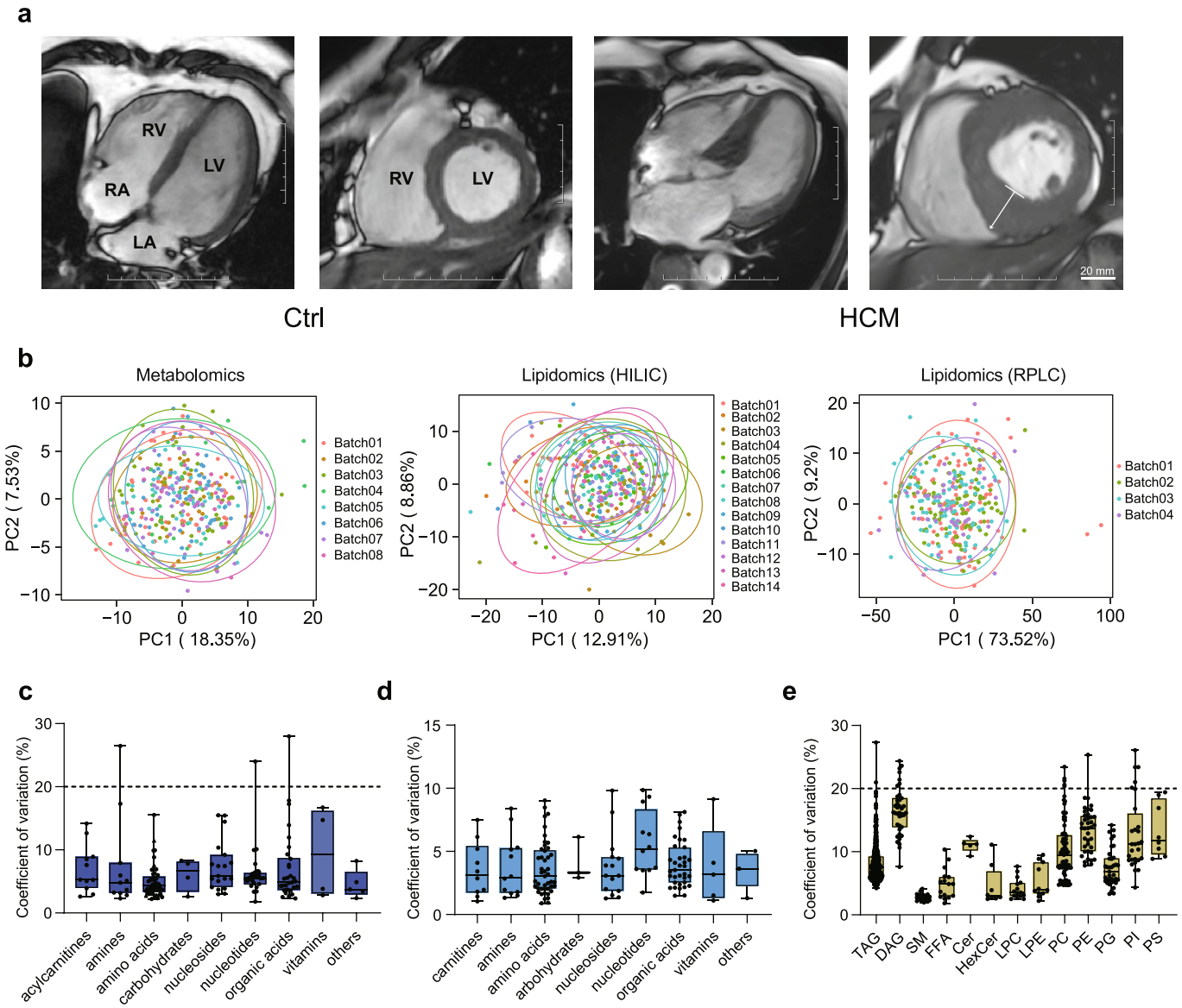

Extended Data Fig. 1 | CMR image of HCM and quality assessments for metabolomics and lipidomics data. a, Representative cardiovascular magnetic resonance (CMR) images of non-HCM (Ctrl) and patients with HCM. The white arrow indicates the maximum thickness of cardiac interventricular septum. LA, left atrium; LV, left ventricular; RA, right atrium; RV, right ventricular. Bar: 20 mm. **b**, Principal component analysis (PCA) across omics assay. Each sample is colored by batch information. c–e, Coefficient of variation for metabolites detected by targeted metabolomics in cardiac tissues (n = 44) (c) and plasma (n = 22) (d) and lipidomics (for TAG, n = 30; for other lipid classes, n = 59) (e) of quality control samples. The box plots visualized as median and 25th and 75th percentiles, with whiskers indicating maximal and minimal values.

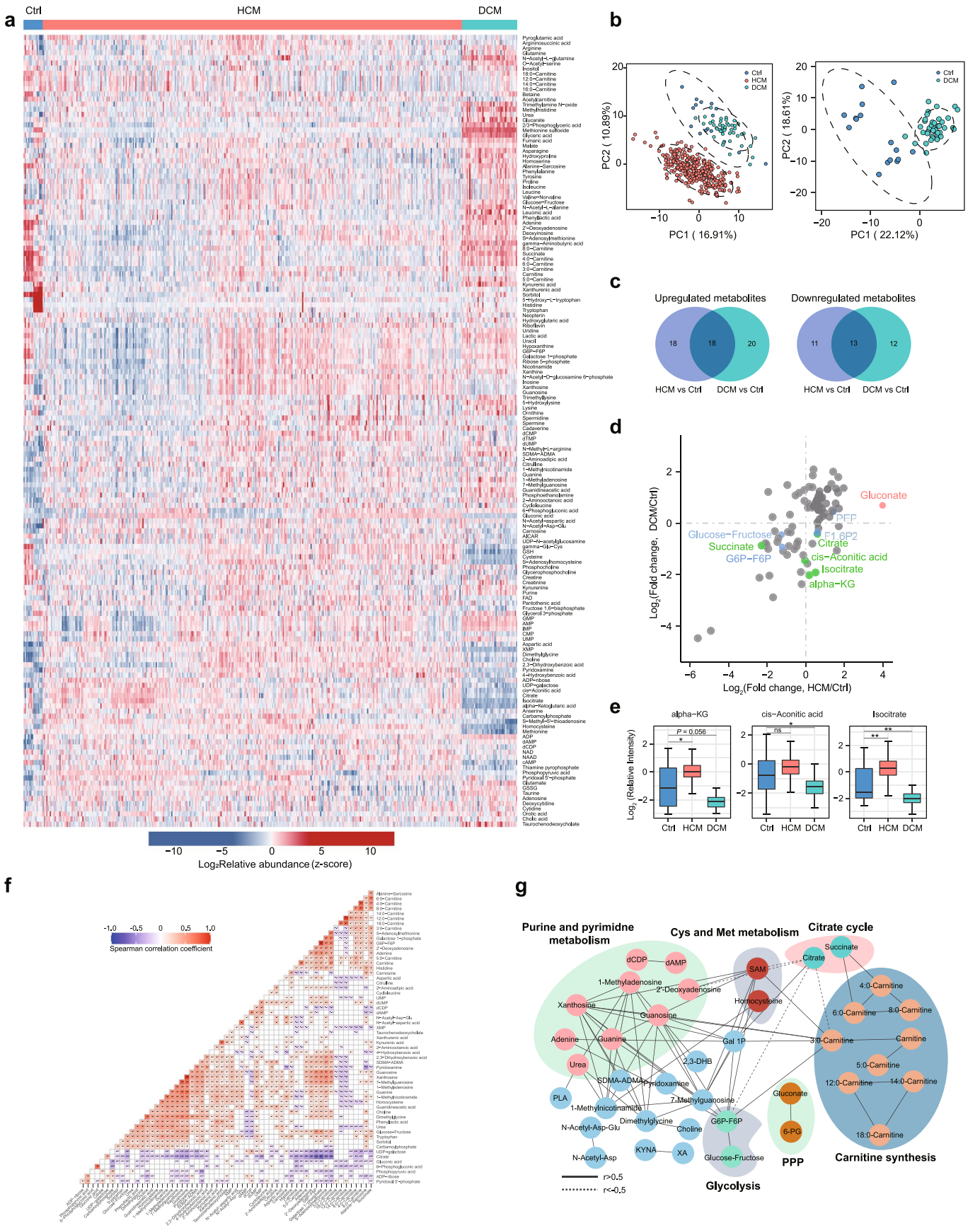

Extended Data Fig. 2 | See next page for caption.

Extended Data Fig. 2 | Overview of metabolomics data in the heart tissues from patients with HCM, related to Fig. 2. a, Heatmap of metabolites relative abundance in non-HCM controls (Ctrl), HCM and DCM patients. **b**, PCA score plot of targeted metabolomics data on non-HCM controls, HCM and DCM patients. **c**, Venn diagram depicting the number of upregulated (left) and downregulated (right) metabolites in HCM and DCM group. **d**, Log2 fold change of differential metabolites in the HCM (x axis) or DCM (y axis) compared to non-HCM controls. **e**, Relative intensity of metabolites involved in TCA cycle in non-HCM controls (n = 16), HCM (n = 349) and DCM patients (n = 46). The box plots visualized as median and 25th and 75th percentiles, with whiskers indicating maximal and minimal values. **f**, Heatmap of spearman correlation coefficient of differential metabolites between HCM patients and non-HCM controls. Only pair metabolites with P value < 0.05 were colored and spearman correlation coefficient are labeled in the relevant box. **g**, Spearman correlation networks of differential metabolites with absolute correlation coefficient greater than 0.5. The solid line represents positive correlation and the dash line represents negative correlation. Statistical analyses were performed by two-sided Mann–Whitney U-test (e). (exact P values are provided in the source data). Asterisks indicate significance as follows: ns $P \geq 0.05$, $^{*}P < 0.05$, $^{**}P < 0.01$.

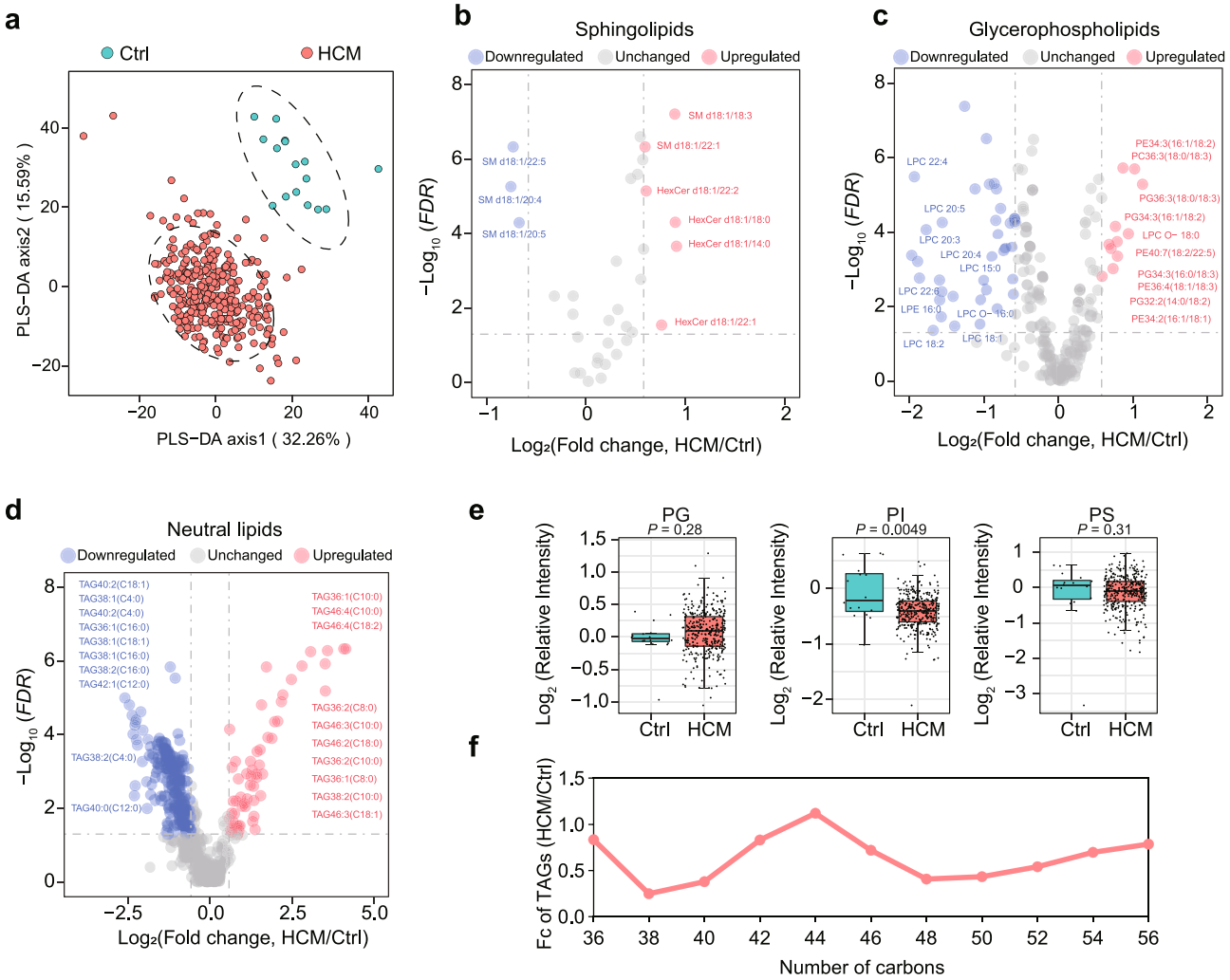

Extended Data Fig. 3 | Overview of lipidomics data in the heart tissues from HCM patients, related to Fig. 3. a, PLS-DA score plot of lipidomics data on HCM patients and non-HCM controls (Ctrl). b-d, Volcano plots of sphingolipids (**b**), glycerophospholipids (**c**) and neutral lipids (**d**) alterations between HCM and non-HCM controls. Significantly upregulated, downregulated (FDR-corrected P value < 0.05, fold change > 1.5 or < 0.67) and unchanged metabolites were colored in red, blue, and gray, respectively. Top 10 most significantly increased or decreased metabolites of fold change in each group are labeled. The horizontal line denotes a FDR cutoff of 0.05, and the vertical lines denote a fold change of 1.5 or 0.67. **e**, Relative intensity of PG, PI and PS in HCM (n = 349) and non-HCM controls (n = 16). The box plots visualized as median and 25th and 75th percentiles, with whiskers indicating maximal and minimal values. **f**, Fold change of TAG with different numbers of carbon between HCM and non-HCM controls. Statistical analyses were performed by two-sided Mann–Whitney U-test (e) and followed by Benjamini–Hochberg correction (b-d).

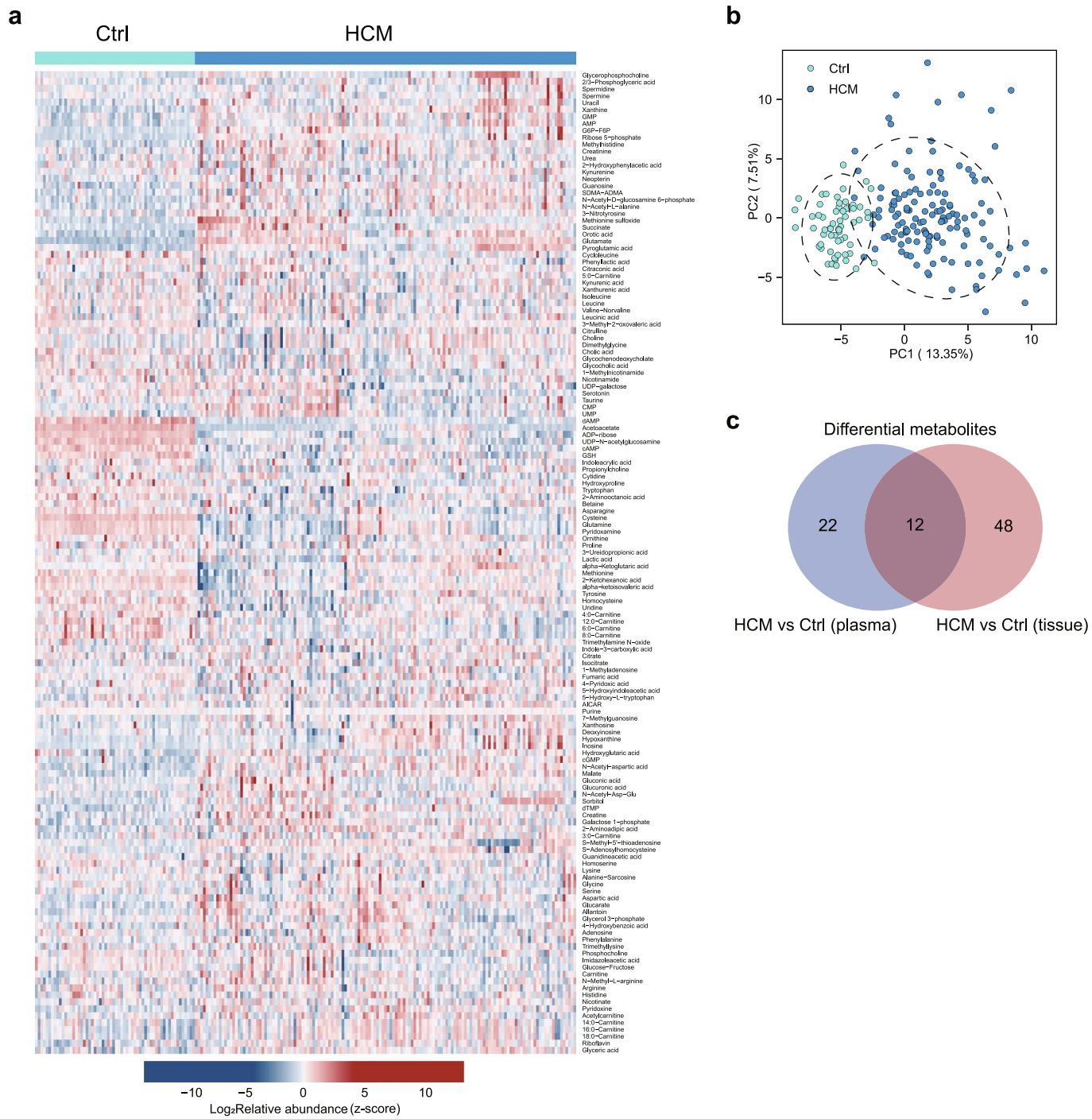

Extended Data Fig. 4 | Metabolic alterations in the plasma of HCM patients, related to Fig. 4. a, Heatmap of metabolites relative abundance in the plasma of non-HCM controls (Ctrl) and HCM patients. **b**, PCA score plot of metabolomics data on the plasma of HCM patients and non-HCM controls. **c**, Venn diagram depicting the number of plasma and tissue differential metabolites between HCM and non-HCM controls group.

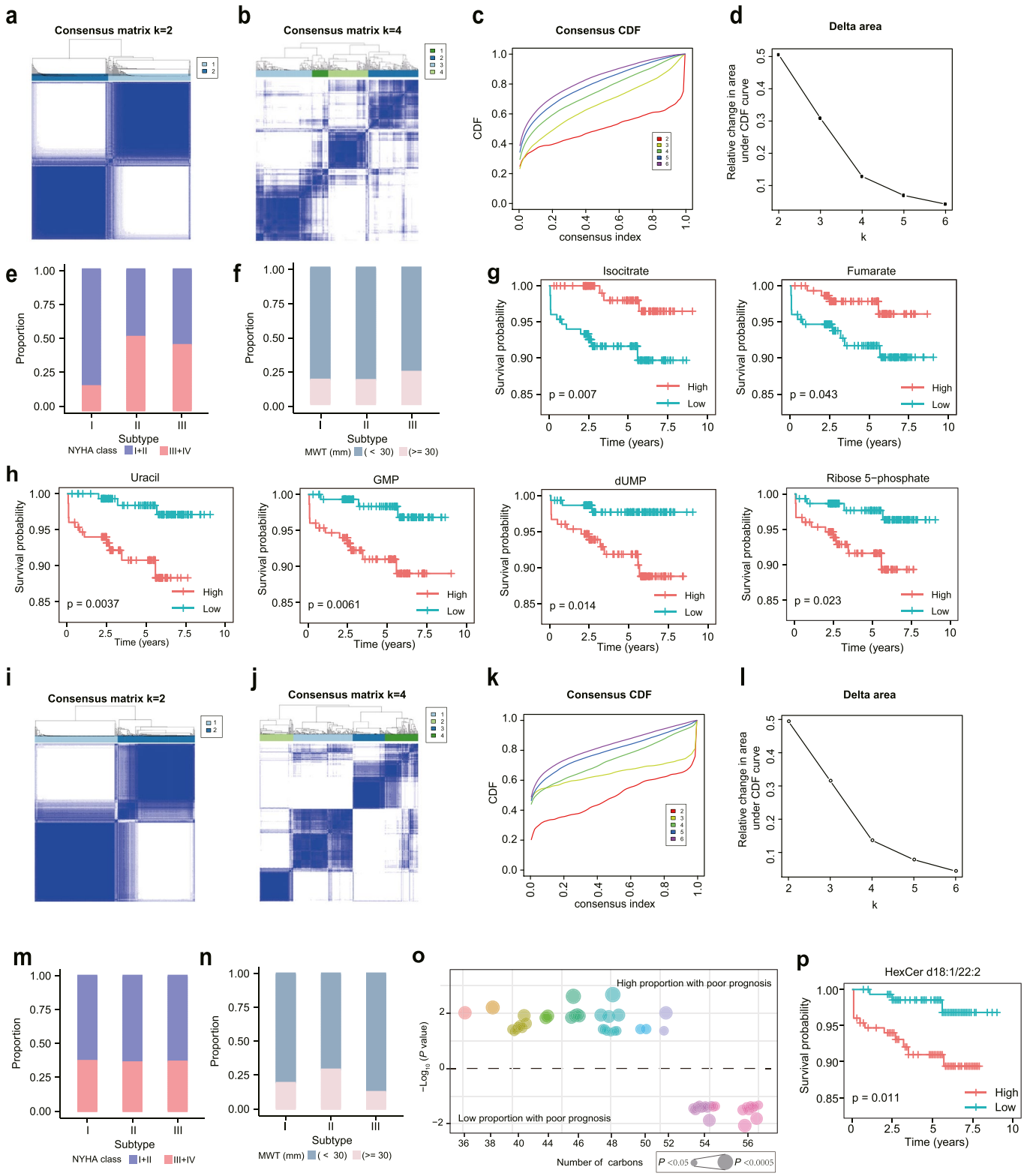

Extended Data Fig. 5 | See next page for caption.

Extended Data Fig. 5 | Metabolic subtyping of HCM and their associations with clinical characteristics, related to Fig. 6. a, **b**, Groups were identified based on metabolomics data of HCM cohort by K-means consensus clustering upon their abundance. Consensus results show consistency for k = 2 (a) and k = 4 (b), the abundance of TAGs was defined as the ratio of each TAG to total TAG abundance in each patient. **c**, Cumulative distribution function (CDF) plot of consensus clustering for HCM patients metabolomics data. **d**, Delta area (change in CDF area) plot of consensus clustering for HCM patients metabolomics data. **e**, **f**, The distribution of HCM patients with different NYHA class (e) and MWT (f) in each individual metabolic subtype. **g**, **h**, Kaplan–Meier curves for overall survival of HCM patients stratified by the relative intensity of isocitrate, fumarate (g), Uracil, GMP, dUMP and R5P (h) (two-sided log-rank test with no multiple comparisons adjustment). The median of metabolite abundances as the cutoff for expression dichotomization. **i**, **j**, Subgroups were identified based on lipidomics data of HCM cohort by K-means consensus clustering upon their abundance. Consensus results show consistency for k = 2 (i) and k = 4 (j). **k**, CDF plot of consensus clustering for HCM patients lipidomics data. **l**, Delta area (change in CDF area) plot of consensus clustering for HCM patients lipidomics data. m, n, The distribution of clinical parameters: NYHA class (**m**) and MWT (**n**) in each individual metabolic cluster. **o**, Bubble plot of significance between TAGs with different numbers of carbon and overall survival. Each dot represents a lipid species. Color coded per TAG with different numbers of carbon. Dot size indicates significance. The abundance of TAGs was defined as the ratio of each TAG to total TAG abundance in each patient. A two-sided log-rank test was used with no multiple comparisons adjustment. **p**, Kaplan–Meier curves for overall survival of HCM patients stratified by the relative intensity of HexCer d18:1/22:2 (two-sided log-rank test). The median of metabolite abundances as the cutoff for expression dichotomization.

nature portfolio

Corresponding author(s): Jizheng Wang, Lei Song, Zeping Hu

Last updated by author(s): Mar 09, 2022

Reporting Summary

Nature Portfolio wishes to improve the reproducibility of the work that we publish. This form provides structure for consistency and transparency in reporting. For further information on Nature Portfolio policies, see our Editorial Policies and the Editorial Policy Checklist.

Statistics

For all statistical analyses, confirm that the following items are present in the figure legend, table legend, main text, or Methods section.

n/a	Confirmed	
☐	☒	The exact sample size (*n*) for each experimental group/condition, given as a discrete number and unit of measurement
☐	☒	A statement on whether measurements were taken from distinct samples or whether the same sample was measured repeatedly
☐	☒	The statistical test(s) used AND whether they are one- or two-sided *Only common tests should be described solely by name; describe more complex techniques in the Methods section.*
☒	☐	A description of all covariates tested
☐	☒	A description of any assumptions or corrections, such as tests of normality and adjustment for multiple comparisons
☐	☒	A full description of the statistical parameters including central tendency (e.g. means) or other basic estimates (e.g. regression coefficient) AND variation (e.g. standard deviation) or associated estimates of uncertainty (e.g. confidence intervals)
☐	☒	For null hypothesis testing, the test statistic (e.g. *F*, *t*, *r*) with confidence intervals, effect sizes, degrees of freedom and *P* value noted *Give P values as exact values whenever suitable.*
☒	☐	For Bayesian analysis, information on the choice of priors and Markov chain Monte Carlo settings
☐	☒	For hierarchical and complex designs, identification of the appropriate level for tests and full reporting of outcomes
☒	☐	Estimates of effect sizes (e.g. Cohen's *d*, Pearson's *r*), indicating how they were calculated

Our web collection on statistics for biologists contains articles on many of the points above.

Software and code

Policy information about availability of computer code

Data collection	The baseline clinical characteristics of patients with HCM were collected at enrollment (i.e. the time of myomectomy). Left ventricle wall thickness, left ventricular outflow tract (LVOT) gradient and left ventricular ejection fraction (LVEF) were all assessed by echocardiography. All patients were followed-up annually until July 2020 by a clinic visit or telephone interview. The follow-up time extended from the first evaluation until death from any cause or the last known contact date. The study end point was cardiovascular deaths, including sudden cardiac death and deaths due to heart failure and stroke. Whole-exome sequencing was performed on Illumina NovaSeq platform. The obtained reads were aligned to the human reference genome and variants were called using Genome Analysis Toolkit (v.3.7). Targeted metabolomics data were collected with triple quadrupole mass spectrometer (Qtrap 6500+, SCIEX). Lipidomics was performed with the Xevo TQ-XS mass spectrometer (Waters). Proteomics data were collected with Q ExactiveTM Plus MS/MS system (Thermo). Western blot gel image was obtained with a chemiluminescent imager (Tanon5200)
Data analysis	SnpEff software (v.4.3) for whole-exome sequencing data analysis MultiQuant software v.3.0 (Sciex) for metabolomics data analysis Skyline software v.4.1 (MacCoss Lab) for lipidomics data analysis Maxquant search engine (v.1.5.2.8) for proteomics data analysis R stat (v.3.6.3) package for Mann-Whitney U test and PCA analysis R clusterProfiler (v.3.12.0) package for KEGG pathway (metabolites) analysis Database for Annotation, Visualization and Integrated Discovery (v6.8) for KEGG pathway (proteins) analysis Cytoscape (v.3.8.0) software for co-expression networks analysis R survival (v.3.1-11) package for survival analysis R survminer (v.0.4.6) package for Kaplan-Meier survival curves analysis Python scikit-learn (v.0.24.1) package for LASSO and random forests analysis Python scikit-survival (v.0.17.1) package for random survival forests analysis

R ConsensusClusterPlus (v.1.48.0) package for K-means consensus clustering analysis
R dunn.test (v.1.3.5) package for Kruskal-Wallis tests with Dunn's multiple comparison test analysis
Excel (version 2016) and GraphPad Prism (v.8.0) for Student's t test analysis

For manuscripts utilizing custom algorithms or software that are central to the research but not yet described in published literature, software must be made available to editors and reviewers. We strongly encourage code deposition in a community repository (e.g. GitHub). See the Nature Portfolio guidelines for submitting code & software for further information.

Data

Policy information about availability of data

All manuscripts must include a data availability statement. This statement should provide the following information, where applicable:

- Accession codes, unique identifiers, or web links for publicly available datasets
- A description of any restrictions on data availability
- For clinical datasets or third party data, please ensure that the statement adheres to our policy

The clinical information of each HCM patient is detailed in Supplementary Table 1. The baseline clinical characteristics for DCM and non-HCM controls are included in Supplementary Table 2. As public sharing of the raw genomic data is restricted by the regulation of the Human Genetic Resources Administration of China, detailed results of whole exome sequencing are included in Supplementary Table 3. Raw metabolomics and lipidomics data are included in Supplementary Table 4, 5 and 6. The MS proteomics raw data is deposited in the ProteomeXchange Consortium (http://proteomecentral.proteomexchange.org) via the iProX partner repository with dataset identifier PXD032097. Source data are provided with this paper.

Field-specific reporting

Please select the one below that is the best fit for your research. If you are not sure, read the appropriate sections before making your selection.

☒ Life sciences ☐ Behavioural & social sciences ☐ Ecological, evolutionary & environmental sciences

For a reference copy of the document with all sections, see nature.com/documents/nr-reporting-summary-flat.pdf

Life sciences study design

All studies must disclose on these points even when the disclosure is negative.

Sample size	No statistical methods were used to pre-determine sample sizes but our sample sizes are similar to those reported in previous publications
Data exclusions	No data were excluded from the analysis.
Replication	Biological replications are as indicated in figure legends and methods. All attempts at replication were successful.
Randomization	For targeted metabolomics, lipidomics and proteomics studies, patient tissue or plasma samples were randomized into different sampling batches. 39 HCM patients used for derivatization were matched with 8 non-HCM controls in age. 16 HCM patients used for western blot were matched with 8 non-HCM controls in age and sex.
Blinding	Each sample was labeled with an numeric ID whose annotation was kept blinded during data collection and analyses.

Reporting for specific materials, systems and methods

We require information from authors about some types of materials, experimental systems and methods used in many studies. Here, indicate whether each material, system or method listed is relevant to your study. If you are not sure if a list item applies to your research, read the appropriate section before selecting a response.

Materials & experimental systems

n/a	Involved in the study
☐	☒ Antibodies
☒	☐ Eukaryotic cell lines
☒	☐ Palaeontology and archaeology
☒	☐ Animals and other organisms
☐	☒ Human research participants
☒	☐ Clinical data
☒	☐ Dual use research of concern

Methods

n/a	Involved in the study
☒	☐ ChIP-seq
☒	☐ Flow cytometry
☒	☐ MRI-based neuroimaging

Antibodies

Antibodies used	The antibody was purchased from the indicated source: Anti-GAPDH (Proteintech, 60004-1-Ig), Anti-G6PD (Sigma, HPA000834), Anti-mouse secondary antibody (CST, 7076S), Anti-rabbit secondary antibody:(7074S, 1:5000).
Validation	The antibody used in this work were purchased from company, and validated by the manufacturers and by extensive use in published work. Anti-GAPDH (Proteintech, 60004-1-Ig) and Anti-G6PD (Sigma, HPA000834) are suitable for western blotting and human samples detection.

Human research participants

Policy information about studies involving human research participants

Population characteristics	Ventricular myocardium samples were obtained from a total of 349 HCM patients (138 Female, 211 Male, Age: 40.0 ± 14.8 years old), 16 non-HCM healthy donors (2 Female, 11 Male, Age: 39.2 ± 18.4 years old, Sex and age of 3 donors were not available due to law for privacy protection) and 46 DCM patients (14 Female, 27 Male, Age: 42.3 ± 14.9 years old, Sex and age of 5 DCM were not available due to law for privacy protection). Plasma samples were collected from 143 HCM patients (53 Female, 90 Male, Age: 44.6 ± 16.5 years old) and 60 non-HCM healthy person (22 Female, 38 Male, Age: 47.8 ± 11.6 years old).
Recruitment	The patient tissue specimens for this study were collected from obstructive HCM patients who underwent a Morrow Septal Myectomy at Fuwai Hospital, Chinese Academy of Medical Sciences and Peking Union Medical College, Beijing, China. Human DCM left ventricular myocardium samples were obtained from patients with dilated cardiomyopathy undergoing cardiac transplantation at Tongji Hospital, Tongji Medical College, Wuhan, China. Left ventricular myocardium of eleven non-HCM were collected from healthy donor hearts that were obtained from explanted normal hearts but not used for transplantation and five were collected from human who donated organs. All of the donors had no history of cardiac diseases. Plasma samples of 143 HCM were collected before surgery and plasma of 60 non-HCM controls were collected from the physical examination population. All samples are free from any potential self-selection bias or other bias.
Ethics oversight	This study was approved by the Ethics Committee of Fuwai Hospital, Chinese Academy of Medical Science and Peking Union Medical College, Beijing, China and Tongji Hospital, Tongji Medical College, Wuhan, China. Written informed consent was obtained from all of the participants or their relatives and and they agree that the data and information obtained from patients could be used in a publication.

Note that full information on the approval of the study protocol must also be provided in the manuscript.